J Comput Aided Mol Des (2013) 27:45–66
DOI 10.1007/s10822-012-9624-4

Computational study of the effects of protein tyrosine nitrations on the catalytic activity of human thymidylate synthase

Adam Jarmuła · Wojciech Rode

Received: 24 May 2012 / Accepted: 6 December 2012 / Published online: 13 December 2012

Abstract Tyrosine nitration is a widespread post-translational modification capable of affecting both the function and structure of the host protein molecule. Enzyme thymidylate synthase (TS), a homodimer, is a molecular target for anticancer therapy. Recently purified TS preparations, isolated from mammalian tissues, were found to be nitrated, suggesting this modification to appear endogenously in normal and tumor tissues. Moreover, human TS (hTS) nitration in vitro led to a by twofold lowered catalytic activity following nitration in average of 1 tyrosine residue per monomer (Dąbrowska-Maś et al. in Org Biomol Chem 10:323–331, 2012), with the modification identified by mass spectrometry at seven different sites (Y33, Y65, Y135, Y213, Y230, Y258 and Y301). In the present paper, combined computational approach, including molecular and essential dynamics and free energy computations, was used to predict the influence on the activity of hTS of nitration of each of the seven tyrosine residues. The simulations were based on the crystal structure of hTS ternary complex with dUMP and Tomudex (PDB code: 1I00), with the Tomudex molecule replaced by the molecule of TS cofactor analogue, tetrahydrofolate. The present results indicate that while with nitration of five out of seven residues (Y33, Y135, Y230, Y258 and Y301), single residue modification appears to have a strong reducing effect on the activity, with the remaining two, Y65 and Y213, no or a weaker influence is apparent. Taken together, these results demonstrate that tyrosine nitrations in the hTS enzyme show clear tendency to influence the structure and dynamics and, in turn, catalytic properties of the host enzyme. These effects are overall distance-dependent.

Keywords Protein tyrosine nitration · Thymidylate synthase · Molecular dynamics · Binding free energy computations · Essential dynamics

Introduction

Thymidylate synthase (TS; EC 2.1.1.45) catalyzes a key step in the biosynthetic pathway of thymidylate (dTMP), i.e., the reductive methylation of 2′-deoxyuridylate (dUMP), with N(5,10)-methylenetetrahydrofolate (meTHF) participating as both the one carbon group donor and reducing agent [1]. The reaction is required for DNA synthesis, therefore its inhibition has long been recognized as a valuable strategy in chemotherapy [2], with some TS inhibitors (5-fluorouracil, Raltitrexed, Pemetrexed) being active forms of approved drugs [3, 4].

Protein tyrosine nitration (PTN), which adds a nitro ($-NO_2$) group at the 3-position of tyrosine's phenolic ring, yielding 3-nitrotyrosine (chemical name: (2S)-2-amino-3-(4-hydroxy-3-nitro-phenyl)propanoic acid), is a post-translational modification (PTM) observed in a large number of proteins, organs and disease conditions [5]. The addition of the $-NO_2$ group to the phenolic ring shifts the pKa of the tyrosine hydroxyl group from 10.1 to 7.2, thus introducing a net negative charge to the nitrated tyrosine at the physiological pH [6]. The latter impacts the local chemical environment, with potential multiple consequences for protein structure and functionality, including generating novel antigenic epitopes, changing enzymatic

Electronic supplementary material The online version of this article (doi:10.1007/s10822-012-9624-4) contains supplementary material, which is available to authorized users.

A. Jarmuła (✉) · W. Rode
Nencki Institute of Experimental Biology, Polish Academy of Sciences, 3 Pasteur St., 02-093 Warszawa, Poland
e-mail: a.jarmula@nencki.gov.pl

activity, modulating signaling and/or metabolic pathways, and several others [7, 8]. Moreover, it has been suggested that this modification may play critical roles in several physiological and pathological processes, including the immune response, cell death, aging, and neurodegeneration [9, 10]. While PTN is a selective process occurring only at specific residues [11, 12], due to an overall low abundance of this modification, the exact sites of in vivo nitration remain usually hard to identify [13, 14].

Recently, highly purified preparations of TS, isolated from calf thymus and L1210 cells, have been found to be nitrated, indicating the modification to take place endogenously in both normal and tumor tissues [15]. Each human, mouse, and *Caenorhabditis elegans* recombinant TS preparation underwent tyrosine nitration, leading to the catalytic efficiency (V_{max}^{app}) by 2-fold lower following nitration of 1 (with human and *C. elegans* TS) or 2 (with mouse TS) tyrosine residues per protein monomer. Mass spectrometry (MS) analysis revealed several TS-derived peptides containing nitro-tyrosines at positions 33, 65, 135, 213, 230, 258, and 301 in the human enzyme (Fig. 1). However, no indications were given about the possible impact of a particular nitration on the enzymatic activity. The present paper attempts to assess at the molecular level potential of each of those nitrations to influence the enzyme's catalytic activity.

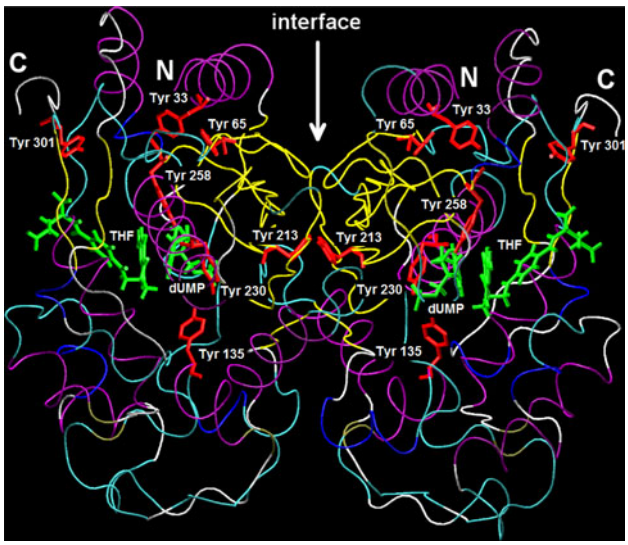

Fig. 1 Tube representation of the dimer structure of hTS with bound dUMP and THF. Coloring according to the secondary structure elements (α-helix: *purple*, 3(10)-helix: *blue*, β-sheet: *yellow*, turn: *cyan*, coil: *white*). N- and C-termini are labelled. Nitrated tyrosine residues are shown as *red sticks* and labelled with sequence numbers. dUMP and THF are shown as *green sticks*

Methods

Molecular dynamics (MD)

Molecular dynamics simulations have been performed in order to comparatively envision the influence of a given tyrosine residue nitration on the catalytic activity of human TS (hTS). The simulations were started from the monomer A of the dimeric crystallographic structure of the ternary complex of hTS with dUMP and Tomudex (PDB code: 1I00) [16], from which the residue numbering used throughout the paper has been adopted. The monomer A of the 1I00 structure has been prepared for the simulations according to the protocol described in Jarmuła et al. [17], with the Tomudex molecule being replaced with the molecule of tetrahydrofolate (THF; close analogue of meTHF), resulting in the hTS-dUMP-THF ternary system. Each time one of the Tyr 33, 65, 135, 213, 230, 258, and 301 residues was substituted at the ortho carbon of the phenolic ring with the $-NO_2$ group, leading to nitrated variants of the hTS-dUMP-THF system. After generating hydrogen atom positions with the *leap* module of AMBER 8 [18], the nitrated systems were solvated in truncated octahedron boxes of TIP3P water molecules [19]. Periodic boundary conditions were applied throughout the simulations. Sodium counterions were added to the systems to neutralize the net charges of the protein and ligands, resulting in the total number of atoms amounting to between 20,970 and 22,176 (depending on the system). All simulations were performed with the *Sander* module of AMBER 8 using the Duan et al. [20] (ff03) force field parameters. The parameters for nitrated tyrosines have been derived from the GAFF force field [21] using the standard procedure available in AMBER (these parameters have been deposited as supplementary material). The partial atomic charges for dUMP and THF (for labeling see Fig. 2) and for nitrated tyrosines were obtained with the RESP method [22, 23] by fitting the electrostatic potentials calculated at the RHF/6-31G* level of theory.

The protocol for energy minimization and molecular dynamics runs was the same as the one used in Jarmuła et al. [17]. Briefly, it consisted of (1) the steepest descent, followed by conjugate gradients energy minimization, (2) gradual heating to 300 K, (3) equilibration for 199 ps, and (4) data collection runs (DCR) for 2,000 ps. The NpT ensemble with the pressure set at 1 atm and temperature at 300 K was used throughout the simulations. A 1 fs time step and the SHAKE algorithm [24] to constrain the length of all bonds involving hydrogen atoms were used. Lennard-Jones and electrostatic interactions were evaluated using the particle-mesh Ewald (PME) method [25, 26]. Coordinates were saved every 1 ps for post-analysis, yielding in total 2,000 frames for each MD data collection run.

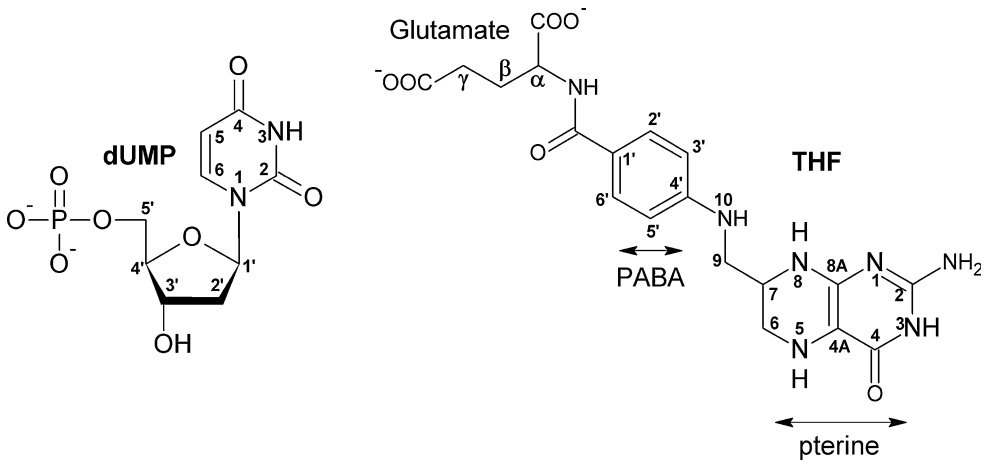

Fig. 2 Labeling schemes for dUMP and THF

The root-mean-square-deviation (RMSD) and root-mean-square-fluctuation (RMSF) of the backbone atoms of the protein were calculated to test the stability of the systems and evaluate the overall structural changes during the simulations, and to assess the per-residue fluctuations, respectively. The percentage of presence of hydrogen bonding interactions was evaluated using the donor–acceptor distance and donor-hydrogen-acceptor angle cut-offs of 3.2 Å and 120°, respectively. Hydrophobic interactions with a cutoff distance of 4 Å were calculated and plotted using the LIGPLOT program [27]. Relative solvent accessibility shown on the LIGPLOT plots was evaluated with the NACCESS program [28]. Average structures from the MD trajectories were calculated using the frames taken from the last 1,200 ps of DCR and applying the protocol used in Jarmuła et al. [17].

Essential dynamics (ED)

Essential dynamics allows identifying concerted motions of proteins that are fundamental to their functions/activities [29, 30]. The method is based on the construction of the covariance matrix of the coordinate fluctuations, which is being diagonalized in order to obtain the eigenvectors and eigenvalues that represent the concerted motions in the system. While the eigenvectors indicate the directions of motion, the corresponding eigenvalues reflect the amplitudes of motion along those directions. The motions along the eigenvectors with large eigenvalues are considered the ones important for the functioning of the system. In the present work, the ED analysis was carried out with the PCAZIP Utilities 3.1 s Principal Component Analysis-based trajectory compression and analysis software [31]. The plots of concerted motions were prepared with the PORCUPINE program [32].

Free energy computations

Binding free energies (ΔG_{bind}) of dUMP and THF in each nitrated system were calculated using the Molecular Mechanics-Generalized Born Surface Area (MM-GBSA) approach [33], applied according to the protocol described in Jarmuła et al. [17]. In short, after discarding water and counterions, molecular mechanics energy contributions to binding for the complex, receptor (protein) and ligand, which can be expressed as the sum of changes in the electrostatic (ΔE_{ele}), van der Waals (ΔE_{vdW}) and internal (ΔE_{int}) energies in the gas-phase, were calculated using a dielectric constant of 1 and an infinite cutoff for all interactions. Polar solvation free energy contributions (ΔG_{GB}) for the complex, receptor and ligand were calculated using a continuum representation of the solvent and the pairwise generalized Born (GB) model of Tsui and Case [34, 35]. Dielectric constants of 1 and 80 were assigned to the solute (protein alone, protein with ligand, or ligand alone) and solvent, respectively. Non-polar solvation free energy contributions (ΔG_{np}) for the complex, receptor and ligand were evaluated from the solvent accessible surface area (SASA) with the LCPO method [36]. All calculations were performed using the tools from AMBER 8 package: *mmpbsa.pl* script and *Sander* program. The solute entropy contributions ($T\Delta S_{solute}$) were not calculated, considering that the normal mode analysis (NMA) of harmonic frequencies, which is often used for this task, tends to provide rough estimates of entropy with large margins of error [37]. Moreover, a high computational cost of NMA is a significant obstacle in the case of larger biomolecules [38], such as those studied here. Finally, the binding free energies obtained in this work have been calculated as: $\Delta G_{bind} = \Delta E_{ele} + \Delta E_{vdW} + \Delta G_{GB} + \Delta G_{np}$.

Results and discussion

RMSD and RMSF

Table 1 presents the RMSDs between various phases of simulations including DCR (represented by structures averaged over the data collection phases), equilibrations and minimizations (represented by structures after the respective phases). The RMSDs between the data collection and equilibration phases (DC w.r.t. EQ) are modest (values between 1.13 and 1.43 Å) and smaller than the RMSDs between equilibration and minimization phases from the same simulations (EQ w.r.t. MIN; values between 1.50 and 1.70 Å), indicating that the duration of equilibrations was sufficient to produce more stable trajectories thereafter (during the data collection phases). The same conclusion was obtained by monitoring the potential (plots deposited as supplementary material) and kinetic energies of the systems (not shown), each of which converged to stable averages before the end of equilibrations. The RMSDs between the data collection and minimization phases (DC w.r.t. MIN) are larger than the corresponding (EQ w.r.t. MIN) RMSDs in four simulations (involving the hTS enzyme nitrated either on Y65, Y135, Y213, or Y230), whereas smaller in other three simulations (with hTS nitrated either on Y33, Y258, or Y301), indicating a drift of the trajectories from the data collection phase away from the coordinates after minimization (the former case), or toward them (the latter case). The plots of RMSDs as a function of time are shown in Figs. 4a, 6a, 7a, 8a, 10a, 11a and 12a. Simulations of the (Y33-NO_2)hTS-dUMP-THF and (Y65-NO_2)hTS-dUMP-THF complexes (Figs. 4a and 6a, respectively) were stable throughout their entire durations, with the mean RMSDs from the 2 ns DCR amounting to 1.12 and 1.06 Å, respectively. The simulations of the (Y213-NO_2)hTS-dUMP-THF, (Y230-NO_2)hTS-dUMP-THF, (Y258-NO_2)hTS-dUMP-THF and (Y301-NO_2)hTS-dUMP-THF complexes (Figs. 8a, 10a, 11a and 12a, respectively) were also overall stable, although their more diverse RMSD profiles in the course of DCR resulted in slightly higher mean RMSDs of 1.32, 1.14, 1.13 and 1.19 Å, respectively. On the other hand, an overall unstable RMSD profile was observed during 2 ns simulation of the (Y135-NO_2)hTS-dUMP-THF complex (Fig. 7a; mean RMSD: 1.41 Å). This simulation was prolonged to 6 ns in search of convergence of RMSD.

Figure 3 presents average RMSFs per residue, calculated from the trajectories of DCR. Individual nitrations do not change local RMSF patterns but influence the magnitudes of fluctuations throughout the structures. In overall, all the systems in the series show similar RMSF profiles, being in qualitative agreement with the experimental B-factors for the crystal structure of the hTS-dUMP-Tomudex complex [16] (not shown). The largest fluctuations correspond to several surface regions of the protein, differing among the series in the amplitudes of the observed maxima. The highest peaks are found for the protein nitrated on Y65 and Y 135 (average residual RMSF of 3.77 and 4.05 Å, respectively); also, not so large but relatively strong fluctuations characterize the protein nitrated on Y230, Y258 and Y213 (average RMSF of 3.35, 3.54 and 3.57 Å, respectively). The protein in other systems from the analyzed series undergoes less intense fluctuations, with Y33 nitration, lack of nitration (native protein) and Y301 nitration causing in this group the largest (an average RMSF of 3.13 Å), medium (an average RMSF of 3.08 Å) and smallest (an average RMSF of 2.68 Å) RMSF, respectively.

Table 1 Backbone RMSD (Å) calculated in different phases of MD simulations

Complex	RMSD			
	MIN w.r.t. CRYST	EQ w.r.t. MIN	DC w.r.t. EQ	DC w.r.t. MIN
hTS-dUMP-THF[a]	0.82	1.34	1.21	1.66
(Y33-NO_2)hTS-dUMP-THF	0.93	1.70	1.15	1.64
(Y65-NO_2)hTS-dUMP-THF	0.91	1.50	1.13	1.62
(Y135-NO_2)hTS-dUMP-THF	0.97	1.61	1.39	1.76
(Y213-NO_2)hTS-dUMP-THF	0.98	1.50	1.43	1.66
(Y230-NO_2)hTS-dUMP-THF	0.91	1.66	1.20	1.74
(Y258-NO_2)hTS-dUMP-THF	1.05	1.53	1.20	1.39
(Y301-NO_2)hTS-dUMP-THF	0.89	1.69	1.19	1.42

EQ, MIN, DC and CRYST denote equilibration, minimization and data collection phases of MD simulations, and the crystal structure of 1I00 (monomer A), respectively

[a] From Jarmuła et al. [17]

Selected criteria to evaluate the PTN impact on the enzymatic activity of hTS

The present assessment of possible impact of each MS-revealed nitration on the enzymatic activity of hTS consists of the following parts: (1) a structural/conformational analysis of the nitrated complexes with an emphasis on the positions adopted in the MD simulations by the ligands, dUMP and THF, including an evaluation of hydrogen bonding and hydrophobic interactions, (2) analysis of protein dynamics in the course of MD simulations using

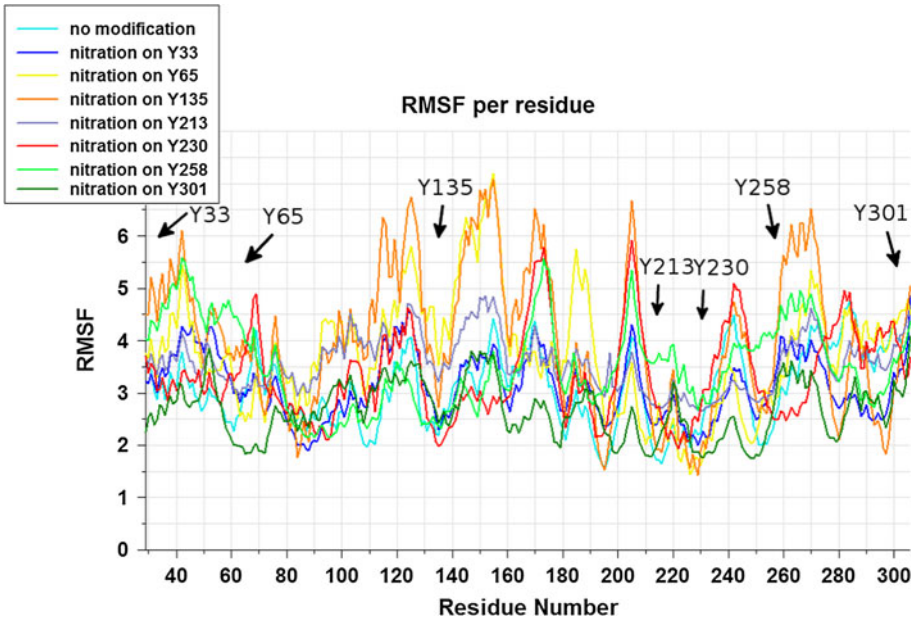

Fig. 3 Average per-residue backbone RMSFs (Å) in unmodified and nitrated hTS complexed with dUMP and THF. Nitration sites are marked with *arrows*

the ED approach, and (3) estimation of binding free energies of the ligands to the host protein in the nitrated complexes.

Essential dynamics

Major concerted motions in the systems were computed with the essential dynamics method. The dominant motions are associated with the first eigenvectors, explaining 20.7–66.2 % of the total variance in the motions. In general, the second and further eigenvectors explain much less variance in the motions; however, in the Y33-, Y65-, Y213- and Y258-nitrated complexes the variance explained by the second eigenvectors amounts to about 10 %, being about 2.0–3.3-fold lower than the variance explained by the corresponding first eigenvectors (Table 2). Time evolution of trajectories projected on the first and, in the cases of complexes nitrated on Y33, Y65, Y213 and Y258, also second eigenvector, have been computed and plotted for each pair composed of nitrated and native systems (except for the plot for the Y258-nitrated system, projections along the second eigenvector are not shown in the paper since they did not contribute meaningful information). The calculated correlation coefficients (r^2) indicate that the motions associated with the first eigenvectors are analogous between hTS-dUMP-THF and each of the following nitrated complexes: (Y33-NO_2)hTS-dUMP-THF, (Y135-NO_2)hTS-dUMP-THF, (Y213-NO_2)hTS-dUMP-THF, and (Y-258-NO_2)hTS-dUMP-THF (Table 3). Lower correlation is observed between hTS-dUMP-THF and (Y65-NO_2)hTS-dUMP-THF, and especially low between hTS-dUMP-THF and each of the two remaining nitrated complexes: (Y230-NO_2)hTS-dUMP-THF and (Y301-NO_2)hTS-dUMP-THF. In addition, the linear regression coefficients (A) indicate that the motions associated with the first eigenvectors are suppressed in Y33-, Y65-, Y213- and Y301-, whereas equal in Y258- and extended in Y135- and Y230-nitrated complexes, as compared to the native complex. Taken together, for such data no clear pattern is apparent (each nitration is affecting differently the dynamics of the hTS protein), so the analysis of concerted motions will be discussed later in the paper individually for each complex.

Table 2 Percentages of variance in the motions explained by the first (1st) and second (2nd) eigenvectors and the ratio between them

Complex	1st eigenvector	2nd eigenvector	1st/2nd ratio
hTS-dUMP-THF[a]	31.1	7.1	4.38
(Y33-NO_2)hTS-dUMP-THF	23.5	10.7	2.20
(Y65-NO_2)hTS-dUMP-THF	20.7	10.2	2.03
(Y135-NO_2)hTS-dUMP-THF	42.7	7.5	5.69
(Y213-NO_2)hTS-dUMP-THF	24.5	9.9	2.47
(Y230-NO_2)hTS-dUMP-THF	66.2	5.0	13.24
(Y258-NO_2)hTS-dUMP-THF	33.7	10.1	3.34
(Y301-NO_2)hTS-dUMP-THF	50.6	7.6	6.66

[a] From Jarmuła et al. [17]

Binding free energies

The binding free energies have been calculated for ensembles of structures collected during last 1,200 ps of DCR. Table 4 presents the free energies of binding of dUMP and THF in the hTS-dUMP-THF and all nitrated complexes. Due to lack of experimental data to compare with, the energies presented herein should be treated as qualitative measures of binding rather than quantitative

Table 3 Correlation and linear regression coefficients (r^2 and A, respectively) between the distributions of the projections of data collection trajectories onto the first eigenvectors for the pairs composed of native and nitrated complexes

Pair of complexes	r^2	A	Comment[a]
Native vs nitrated on Y33	0.81	0.77	Strongly analogous; suppressed
Native vs nitrated on Y65	0.55	0.58	Poorly correlated; strongly suppressed
Native vs nitrated on Y135	0.69	1.20	Analogous; extended
Native vs nitrated on Y213	0.71	0.79	Analogous; suppressed
Native vs nitrated on Y230	0.42	1.49	Very poorly correlated; strongly extended
Native vs nitrated on Y258	0.71	1.00	Analogous; equally strong
Native vs nitrated on Y301	0.34	0.94	Very poorly correlated; slightly suppressed

[a] Characteristics of the motions along the first eigenvectors in nitrated with respect to native complexes in view of, successively, r^2 and A

ones. The results indicate that the binding of dUMP is favored in the native system with respect to each nitrated derivative. The calculated binding free energies of dUMP in the nitrated complexes span a relatively broad range, differing from the corresponding binding free energy in the native complex by 1.57 to 9.21 kcal/mol (nitrations on Y65 and Y258, respectively). These free energies, compared to that of dUMP in the native complex, allow to classify all the nitrated complexes into two groups: (1) the one with the binding of dUMP being disfavored very strongly (by above 7 kcal/mol), including (Y135-NO_2)hTS-dUMP-THF, (Y258-NO_2)hTS-dUMP-THF and (Y301-NO_2)hTS-dUMP-THF, and (2) the one with the binding of dUMP being disfavored less substantially (by up to 4 kcal/mol), including (Y33-NO_2)hTS-dUMP-THF, (Y65-NO_2)hTS-dUMP-THF, (Y213-NO_2)hTS-dUMP-THF and (Y230-NO_2)hTS-dUMP-THF. In the case of THF, the binding is still favored in the native compared to the nitrated systems, with a single exception being the binding in the (Y65-NO_2)hTS-dUMP-THF complex, calculated to be the most favorable in the studied series. In the rest of the nitrated complexes, the binding of THF is disfavored to a small to medium extent (up to 3.1 kcal/mol; nitrations on Y33, Y213, Y230, Y258 and Y301) or more substantially (by 5.4 kcal/mol; nitration on Y135). Inspection of individual contributions shows that the variation in the binding free energies of both dUMP and THF depends on (1) the balance between the ΔE_{ele} and ΔG_{GB} terms (represented in Table 4 as $\Delta G_{GB,ele}$), and (2) differences in the van der Waals energies (ΔE_{vdW}).

Nitration on Y33

Compared with the superimposed average structure of the native hTS-dUMP-THF complex, the average structure of the (Y33-NO_2)hTS-dUMP-THF complex reveals different positions of the dUMP and THF molecules in the active site of the protein (Fig. 4b). The latter is reflected in particular by the lack of the parallel alignment between the dUMP pyrimidine and THF pterine rings, being in contrast to the unperturbed course of the TS-catalyzed reaction, with the two rings being properly aligned and engaged in covalent interaction with each other [1]. Resulting in the lack of favorable ring-stacking interaction between the rings, this effect lowers the stabilization of both ligand molecules. The new position of the pyrimidine ring is maintained through the changes in hydrogen bonding to the O4 atom, which, upon shifting, gains the H-bonds to the side chains of Tyr 135 (majorly in the simulation) and His 196 (both side chains moved and rotated for better fit, compared to their positions in hTS-dUMP-THF), while loosing the H-bond with Asn 226 (see Table 5). The position of the pterine and aromatic (PABA) rings of THF in the Y33-nitrated complex is secured by favorable hydrophobic interactions with neighboring residues of Trp 109, Leu 221, Phe 225 and Ile 108 (Fig. 4c). This hydrophobic interface is less extensive for the pterine and more extensive for the PABA ring, as compared with the corresponding interface in the hTS-dUMP-THF complex (Fig. 5a). At the same time, the hydrogen bonding interface between the THF molecule and protein molecule is comparable and even more extensive in the nitrated compared to native complex. The positions of dUMP and THF in the hTS active site let to determine distances between the pairs of atoms engaged in bonding upon activation of the native enzyme-substrate-cofactor complex: dUMP C6 and the γS of catalytic Cys 195 (bonded directly), and dUMP C5 and THF N5 (bonded through the methylene bridge). Those distances in the Y33-nitrated and native complexes are 3.33 and 4.83 Å, and 3.60 and 4.02 Å, respectively (Table 6). The difference in the C5 (dUMP)–N5 (THF) distances reflects the disturbed alignment of the dUMP pyrimidine and THF pterine rings in the nitrated state, compared to the correct one in the native state.

The results of binding free energies qualitatively confirm the observations from the structural analysis of the (Y33-NO_2)hTS-dUMP-THF complex, indicating the molecules of dUMP and THF to have less favorable free energies of binding compared to the corresponding free energies in the hTS-dUMP-THF complex (Table 4). The

Table 4 Binding free energies and free energy contributions (kcal/mol) for the native and nitrated complexes of hTS (values in parentheses are standard deviations)

Complex	ΔE_{ele}	ΔE_{vdW}	ΔG_{GB}	ΔG_{np}	$\Delta G_{GB,ele}$	ΔG_{bind}
hTS-dUMP-THF[a]						
dUMP	−98.79 (18.51)	−33.07 (3.63)	92.75 (16.41)	−4.46 (0.12)	−6.04 (5.26)	−43.57 (3.77)
THF	−46.20 (26.29)	−45.95 (2.57)	67.76 (25.25)	−5.96 (0.28)	21.56 (3.06)	−30.35 (3.42)
Nitrated on Y33						
dUMP	−58.17 (17.58)	−31.30 (3.88)	54.40 (15.32)	−4.67 (0.11)	−3.78 (5.60)	−39.74 (4.50)
THF	−33.08 (43.61)	−45.15 (3.96)	55.24 (38.85)	−6.41 (0.26)	22.17 (6.31)	−29.39 (5.07)
Nitrated on Y65						
dUMP	−60.95 (17.06)	−33.49 (3.55)	57.06 (12.84)	−4.62 (0.13)	−3.89 (6.34)	−42.00 (4.93)
THF	−60.38 (42.76)	−41.27 (3.80)	74.78 (38.71)	−6.07 (0.34)	14.40 (5.15)	−32.94 (3.88)
Nitrated on Y135						
dUMP	−25.89 (17.49)	−27.17 (4.33)	21.28 (14.51)	−4.47 (0.15)	−4.61 (5.82)	−36.26 (4.53)
THF	−48.21 (33.71)	−34.14 (6.96)	62.76 (30.88)	−5.34 (0.66)	14.56 (4.58)	−24.92 (4.83)
Nitrated on Y213						
dUMP	−30.40 (23.27)	−32.78 (3.63)	27.08 (20.60)	−4.43 (0.10)	−3.32 (5.10)	−40.54 (4.12)
THF	−14.70 (43.76)	−42.99 (3.25)	34.16 (41.57)	−5.95 (0.45)	19.46 (4.72)	−29.48 (4.17)
Nitrated on Y230						
dUMP	−73.59 (13.90)	−31.52 (4.19)	68.73 (11.93)	−4.77 (0.18)	−4.86 (5.09)	−41.16 (4.21)
THF	23.80 (80.28)	−33.22 (4.90)	−13.63 (78.55)	−5.07 (0.53)	10.16 (3.76)	−28.13 (5.95)
Nitrated on Y258						
dUMP	−32.91 (19.49)	−27.20 (4.64)	30.42 (17.20)	−4.67 (0.16)	−2.49 (6.06)	−34.36 (4.62)
THF	−52.85 (40.05)	−30.32 (7.20)	61.00 (36.07)	−5.08 (0.43)	8.15 (5.84)	−27.25 (5.51)
Nitrated on Y301						
dUMP	−61.56 (15.44)	−30.20 (4.47)	61.26 (13.16)	−4.48 (0.09)	−0.29 (5.01)	−34.98 (4.44)
THF	−58.12 (39.14)	−37.13 (4.25)	71.88 (36.65)	−5.76 (0.59)	13.76 (4.75)	−29.14 (6.66)

ΔE_{int} are not included in Table 4 because they amount to zero in the single trajectory approach; $\Delta E_{GB,ele}$ is the sum of changes in the gas-phase electrostatic energy (ΔE_{ele}) and the polar solvation free energy (ΔG_{GB})

[a] From Jarmuła et al. [17]

difference is larger for dUMP than THF (3.83 and 0.96 kcal/mol, respectively). Inspection of the free energy contributions shows that while the binding of dUMP and THF in the native complex strongly benefits from the favorable ΔE_{ele} contributions, the binding in the Y33-nitrated complex benefits also strongly, but not sufficiently for compensation, due to less unfavorable ΔG_{GB} free energies. In addition, the more favorable binding of both ligands in the native complex benefits from more favorable ΔE_{vdW} contribution. On the other hand, the ΔG_{np} contributions slightly favor the binding of the ligands in the Y33-nitrated complex.

The dominant concerted motions in hTS-dUMP-THF and (Y33-NO_2)hTS-dUMP-THF are shown in Figs. 5b and 4d, respectively. Both motions are strongly analogous, with the motion in the Y33-nitrated system being suppressed compared with that in the native system (see Table 3). The motions differ in their moving directions on the left flank of the entrance to the active site pocket, with the motion in the native system extending to the inside, whereas that in the Y33-nitrated system to the outside of the pocket. This is demonstrated by elongated distances between the left and right flanks of the active site entrance in the nitrated state, for example, 14.8 Å between the Cα atoms of two residues on the opposite sites of the entrance, Ser 120 and Gly 52, compared to 10.2 Å in the native state. Since the motions around the entrance contribute (together with the movement of the C-terminus and overall tightening of the active site) to the closing/opening of the active site pocket [39], therefore the dominant motion observed in the Y33-nitrated protein suggests a possible hindrance in the closing of the pocket in the course of the formation of the active enzyme-substrate-cofactor complex, with such effect potentially affecting the catalytic reaction (see also relevant discussion in Jarmuła et al.) [17].

It should be added that expression of thymidylate synthase carrying Y33H mutation has been shown to confer FdUrd resistance to the colonic tumor cell line HCT1 16,

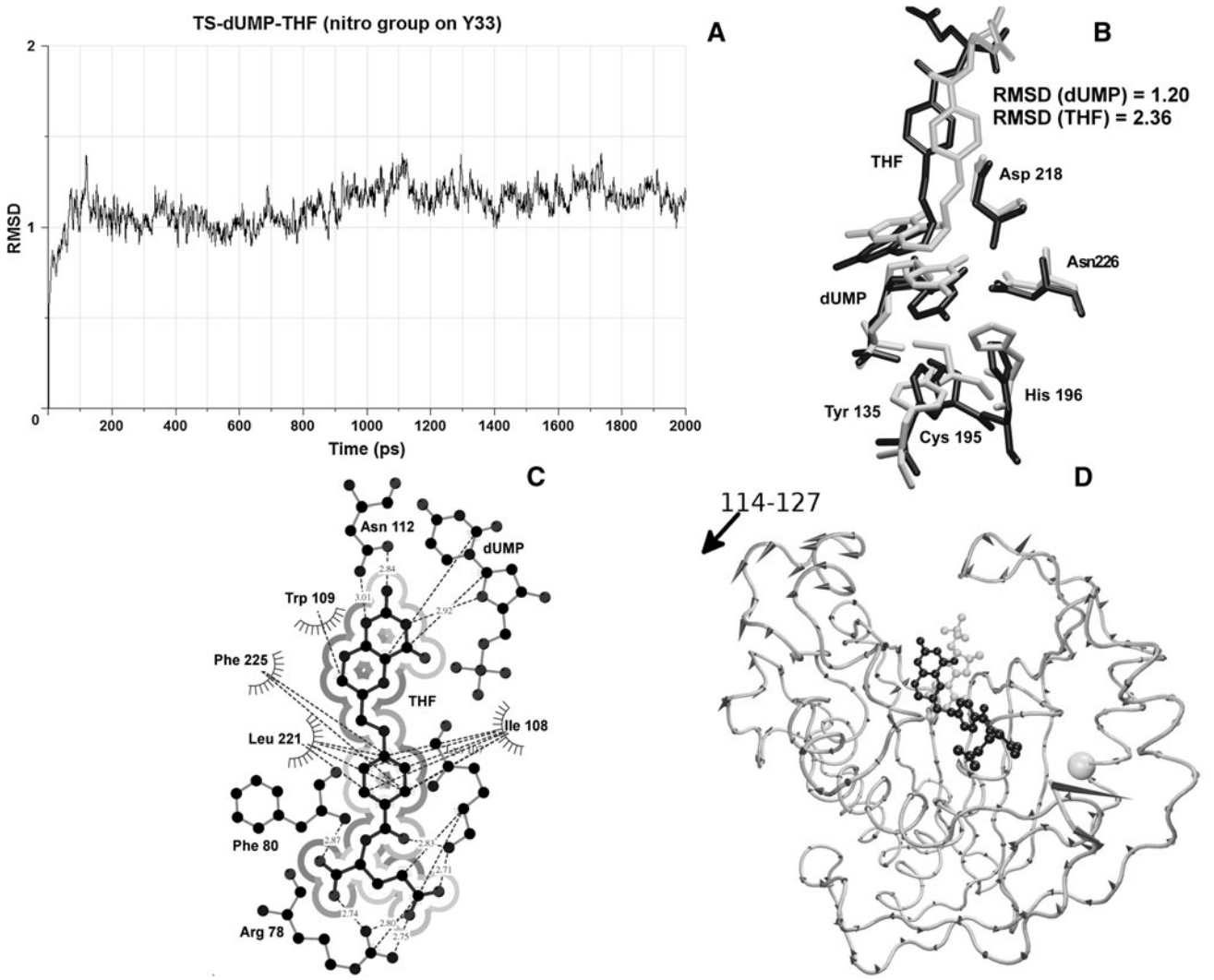

Fig. 4 **a** Time evolution of backbone RMSD (Å) from the structure after equilibration during 2,000 ps data collection MD simulation of (Y33-NO_2)hTS-dUMP-THF; **b** Superimposition of the average structures of hTS-dUMP-THF (*light*) and (Y33-NO_2)hTS-dUMP-THF (*dark*). Shown are the active site residues forming hydrogen bonds with the pyrimidine ring of dUMP, catalytic Cys 195, dUMP and THF. RMSDs (Å) are calculated for all heavy atoms in dUMP and THF. This figure as well as Figs. 6b, 7b, 8b, 9, 10b, 11b and 12b were prepared with VMD [54]; **c** LIGPLOT drawing of the hydrophobic interactions THF-dUMP and THF-protein in (Y33-NO_2)hTS-dUMP-THF. Solvent accessibility around the molecule is shown in *gray scale* from brightest (highly accessible atoms) to darkest (buried atoms); **b** and **c** Hydrogen atoms are omitted for clarity; **d** Concerted motions associated with the first eigenvector in (Y33-NO_2)hTS-dUMP-THF. dUMP and THF are shown respectively as *light* and *dark ball* and *sticks*. Tyr 33 is shown as a *sphere*. Concerted motions are shown as *cones* representing the product of the first eigenvector and first eigenvalue

with the His 33, compared to Tyr 33, enzyme form showing similar K_m values for dUMP and meTHF, but significantly higher k_{cat} value in the TS reaction. However, additional studies on the Phe 33 enzyme revealed the latter effect to be due to the presence of His 33, rather than the absence of Tyr 33 [40]. Also worthy to note are the findings by Cardinale et al. [41] showing that mutation of a nearby residue in the (Gly29–Gly44) α-helix, E30W, perturbs the dynamics and hydrogen-bonding networks of hTS, thus modulating binding of the cofactor and catalysis.

Verdict Nitration on Y33 is expected to significantly reduce the enzymatic activity of hTS.

Nitration on Y65

Compared with the average structure of hTS-dUMP-THF, the average structure of (Y65-NO_2)hTS-dUMP-THF reveals similar, yet somewhat different positions of the dUMP and THF molecules in the protein active site (Fig. 6b). Although slightly rotated with respect to each other, the pyrimidine rings of dUMP are not markedly deviated from parallel placement in the two structures. On the other hand, the pterine ring of THF in the nitrated, compared to unmodified complex, shows a more different placement, being shifted and twisted more distinctly. As a

Table 5 Hydrogen bond occupancies obtained in the courses of DCR

Complex	Hydrogen bond occupancies (%)					
	O2–Asp 218	N3-H–Asn 226	O4–Asn 226	O4–Tyr 135	O4–His 196	O4–Cys 195
hTS-dUMP-THF[a]	64.9	92.7	97.4	0.3	–	–
Nitrated on Y33	2.2	64.3	2.8	79.9	18.5	–
Nitrated on Y65	70.5	77.7	71.1	5.9	–	–
Nitrated on Y135	78.0	71.2	85.6	–	49.9	–
Nitrated on Y213	72.6	73.0	75.3	19.2	2.2	–
Nitrated on Y230	71.3	88.0	84.3	20.8	6.9	–
Nitrated on Y258	37.3	80.6	77.2	9.0	13.6	1.4
Nitrated on Y301	87.2	77.6	98.7	–	–	–

Shown are the interactions between the O2, O4 and N3-H atoms/groups of the pyrimidine ring of dUMP and the protein residues of D218, N226, Y135, H196 and C195

[a] From Jarmuła et al. [17]

result, the pyrimidine and pterine rings in the Y65-nitrated system deviate, although only moderately, from the parallel alignment observed in the native complex. In accord with its only slightly changed position, the pyrimidine ring in (Y65-NO_2)hTS-dUMP-THF maintains majorly in the simulation all hydrogen bonds that were present in hTS-dUMP-THF (Table 5). New positions of the pterine and PABA rings of THF in the nitrated system are secured by favorable hydrophobic interactions with the protein residues of Trp 109, Gly 222, Ile 108, Phe 225 and Leu 221 (with this hydrophobic interface being even tighter than that in hTS-dUMP-THF), as well as—only pterine—by partially preserved ring-stacking with the pyrimidine ring of dUMP, with the latter effect moderately stabilizing the both interacting rings (Fig. 6c). In addition, the position of THF in the Y65-nitrated complex is maintained through a few hydrogen bonds formed by certain heterocyclic atoms of the pterine ring with Asn 112 and Tyr 258. Finally, the C6 (dUMP)–γS (Cys 195) and C5 (dUMP)–N5 (THF) distances are similar in the nitrated, compared to native state (Table 6), reflecting again the similar positions of dUMP and THF in both states.

In (Y65-NO_2)hTS-dUMP-THF, compared to hTS-dUMP-THF, the binding free energies of dUMP and THF predict the binding of dUMP to be unfavorable by about 1.5 kcal/mol, with the binding of THF being favorable by about 2.5 kcal/mol (Table 4). These results qualitatively agree with the observations from structural analysis,

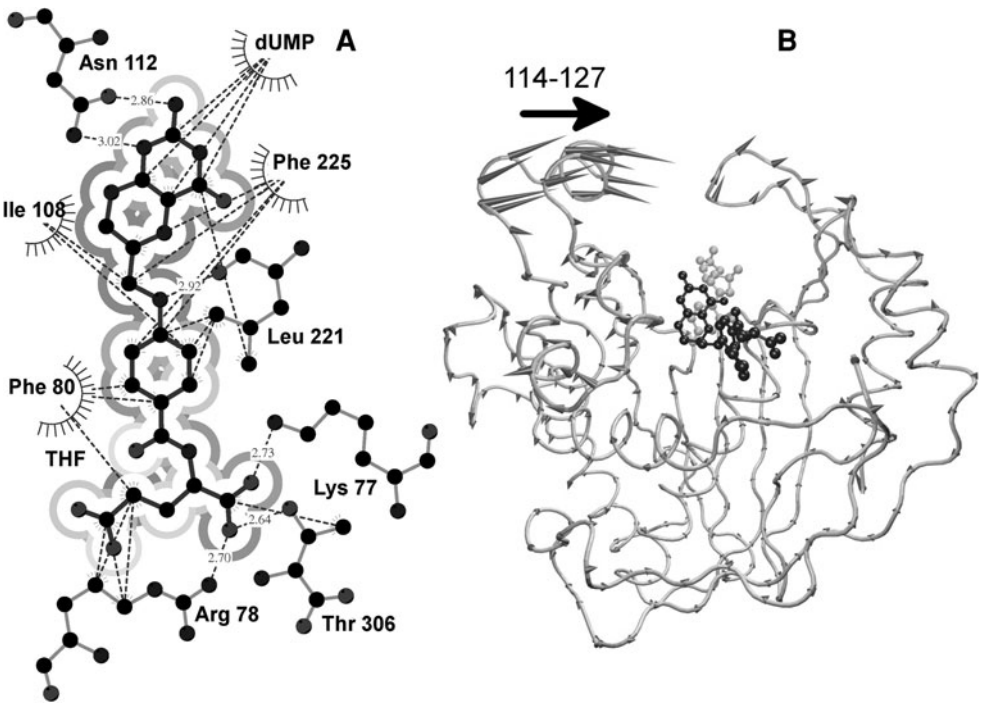

Fig. 5 **a** LIGPLOT drawing of the hydrophobic interactions THF-dUMP and THF-protein in hTS-dUMP-THF. Solvent accessibility around the THF molecule is shown in *gray scale* from brightest (highly accessible atoms) to darkest (buried atoms). Hydrogen atoms are omitted for clarity; **b** Concerted motions associated with the first eigenvector in hTS-dUMP-THF. dUMP and THF are shown respectively as *light* and *dark ball* and *sticks*. Concerted motions are shown as *cones* representing the product of the first eigenvector and first eigenvalue

Table 6 Selected distances in the average structures from the last 1,200 ps of DCR

Complex	Distances (Å)			
	C6 (dUMP)–γS (Cys 195)	C5 (dUMP)–N5 (THF)	N (–NO_2)–centroid (dUMP)[b]	N (–NO_2)–centroid (THF)[c]
hTS-dUMP-THF[a]	3.60	4.02	–	–
Nitrated on Y33	3.33	4.83	12.66	13.02
Nitrated on Y65	3.36	4.12	18.15	19.75
Nitrated on Y135	3.61	6.11	6.85	11.01
Nitrated on Y213	3.84	3.56	12.01	15.28
Nitrated on Y230	3.36	4.91	11.72	17.05
Nitrated on Y258	3.48	6.35	7.80	5.84
Nitrated on Y301	3.79	4.36	19.48	20.23

[a] From Jarmuła et al. [17]

[b] The distance from the nitrogen atom in the –NO_2 group to the centroid of the pyrimidine ring in dUMP

[c] The distance from the nitrogen atom in the –NO_2 group to the centroid of the pterine ring in THF

indicating the molecules of dUMP and THF to be well stabilized in the active site of the Y65-nitrated complex. Inspection of the free energy contributions shows that the binding of dUMP in the native complex benefits strongly from favorable ΔE_{ele} contribution, whereas the binding in the Y65-nitrated complex gains a similarly large, but not sufficient for full compensation, free energy bonus from less unfavorable ΔG_{GB} contribution (the balance of both contributions may be seen in Table 4 in the values of $\Delta G_{GB,ele}$). Interestingly, the binding of THF shows a "reverse" pattern of contributions, with the native and nitrated state bindings being favored, respectively, by ΔG_{GB} and ΔE_{ele} (the effect of the latter being two-fold stronger). In addition, the binding of THF in the native state benefits by about 4.7 kcal/mol due to more favorable ΔE_{vdW} contribution, reducing the overall free energy benefit of the binding in the nitrated state to about 2.5 kcal/mol.

The dominant concerted motion in (Y65-NO_2)hTS-dUMP-THF, shown in Fig. 6d, is poorly correlated with the dominant motion in the native complex hTS-dUMP-THF and, compared to the latter, strongly suppressed (cnf. Fig. 5b and Table 3). Considering these characteristics, and especially a poor correlation between the both mentioned motions, and upon inspecting the visual appearance of the motion in the nitrated state, the latter motion does not seem to have any particular relevance to the catalytic function of the protein. This motion is strongest in the surface regions of hTS, where it is represented by both horizontal (directed inward, toward the center of the protein) and vertical components.

Verdict Nitration on Y65 appears to have only minor or no effect at all on the enzymatic activity of hTS.

Nitration on Y135

Superimposition of the average structures of hTS-dUMP-THF and (Y135-NO_2)hTS-dUMP-THF indicates moderately and substantially different positions of the dUMP and THF molecules, respectively, and particularly their pyrimidine and pterine rings, respectively, in the latter compared to the former complex (Fig. 7b). The new position of the pyrimidine ring is maintained through the hydrogen bonds between O4 and the protein residues of Asn 226 (preserved, similarly as in the native system, majorly in the simulation) and His 196 (new contact maintained throughout approximately half of the simulation) as well as between N3-H and Asn 226, and O2 and Asp 218 (both contacts preserved in roughly similar proportions as in the native system, i.e. majorly in the simulation) (Table 5). The new binding position of THF is stabilized through several hydrophobic contacts between the PABA and pterine rings and the protein residues of Ile 108, Phe 80, Phe 225, Leu 221 and Gly 222 (Fig. 7c). This interface is not very extensive (except of the six contacts between PABA and Ile 108), for example, it entirely lacks contacts to the two carbon atoms (C4 and C6) of the pterine ring. Moreover, in its new position, the THF molecule lacks stabilization from hydrogen bonds. The pyrimidine and pterine rings are not stabilized by each other, as they lack the proper, parallel alignment, being instead twisted and largely shifted away relative to each other, with the latter reflected in a large C5 (dUMP)–N5 (THF) distance of 6.11 Å, compared to 4.02 Å in the native state (Table 6). The effect is substantial due to a small distance between Tyr 135 and dUMP (Table 6), with a strong electrostatic repulsion between the nitro group of Tyr 135 and the double negatively charged phosphate group of dUMP, which in the average structure of the nitrated system are located about 9 Å from each other (not shown), forcing the phosphate to move away from its position in the native system by about 1.0–1.5 Å and so contributing to the positional/conformational change of the dUMP molecule. The latter would cause the loosening/breaking of the pyrimidine-pterine ring-stacking, facilitating a concurrent substantial change in the conformation of the THF molecule (Fig. 7b).

The binding free energies of dUMP and THF in the (Y135-NO_2)hTS-dUMP-THF complex are largely different

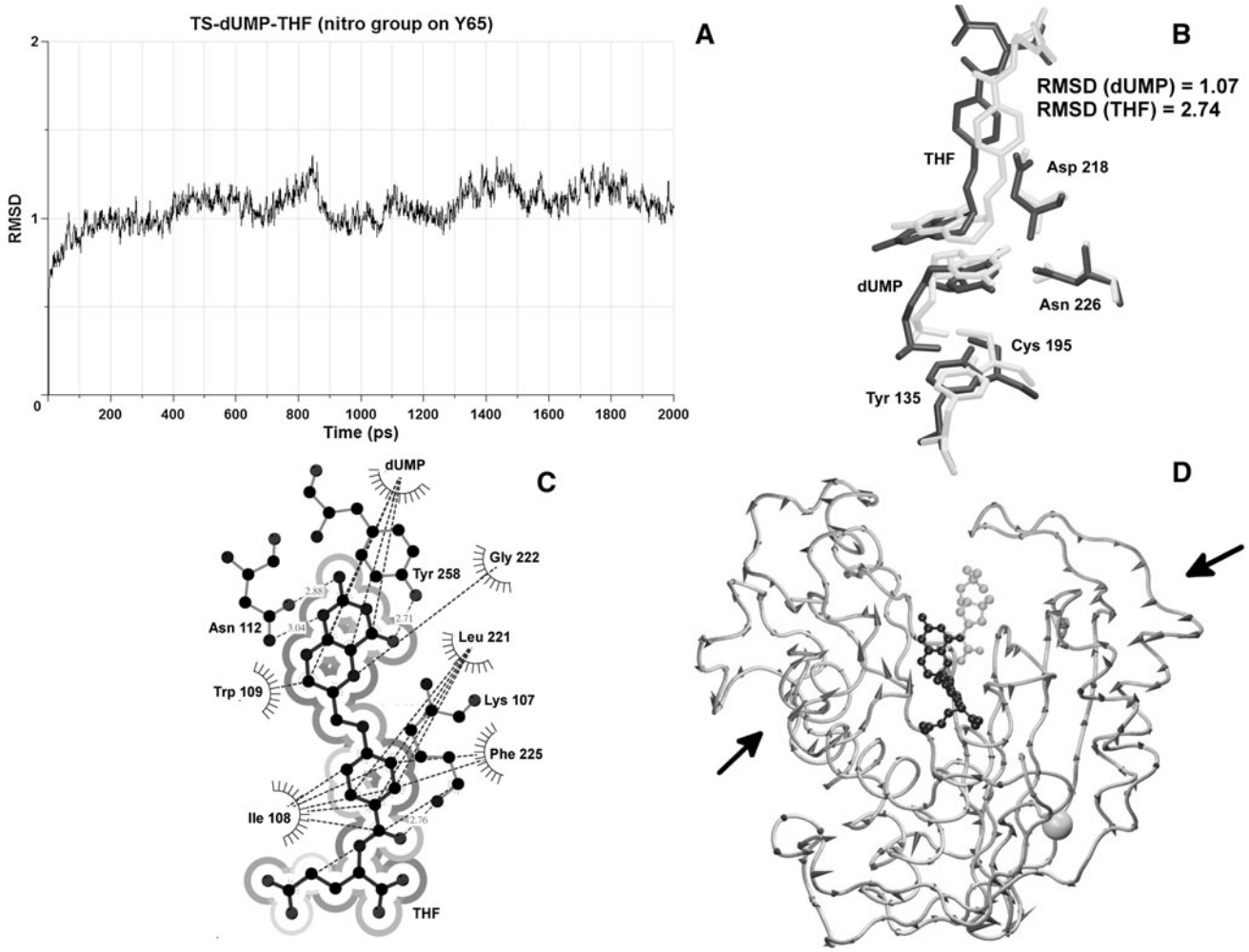

Fig. 6 **a** Time evolution of backbone RMSD (Å) from the structure after equilibration during 2,000 ps data collection MD simulation of (Y65-NO_2)hTS-dUMP-THF; **b** Superimposition of the average structures of hTS-dUMP-THF (*light*) and (Y65-NO_2)hTS-dUMP-THF (*dark*). Shown are the active site residues forming hydrogen bonds with the pyrimidine ring of dUMP, catalytic Cys 195, dUMP and THF. RMSDs (Å) are calculated for all heavy atoms in dUMP and THF. **c** LIGPLOT drawing of the hydrophobic interactions THF-dUMP and THF-protein in (Y65-NO_2)hTS-dUMP-THF. Solvent accessibility around the THF molecule is shown in *gray scale* from brightest (highly accessible atoms) to darkest (buried atoms); **b** and **c** Hydrogen atoms are omitted for clarity; **d** Concerted motions associated with the first eigenvector in (Y65-NO_2)hTS-dUMP-THF. dUMP and THF are shown respectively as *light* and *dark ball* and *sticks*. Tyr 65 is shown as a *sphere*. Concerted motions are shown as *cones* representing the product of the first eigenvector and first eigenvalue

from the corresponding free energies in the hTS-dUMP-THF complex, predicting much weaker bindings in the nitrated state (Table 4). These results are in a good qualitative agreement with the results of structural analysis of the (Y135-NO_2)hTS-dUMP-THF complex, confirming weaker stabilization of dUMP and THF molecules in the nitrated state. Inspection of the binding free energy contributions indicates the imbalance in the energies of electrostatic origin to promote the binding of dUMP in the native, while THF in the nitrated state (see ΔE_{ele}, ΔG_{GB} and $\Delta G_{GB,ele}$ in Table 4). The ΔE_{vdW} contributions promote strongly the bindings in the native state, causing the final binding free energies to be unfavorable in the nitrated state by about 7.3 kcal/mol for dUMP and 5.4 kcal/mol for THF.

The dominant concerted motion in (Y135-NO_2)hTS-dUMP-THF, shown in Fig. 7d, is analogous with, and extended, compared to the corresponding motion in the native system (cnf. Table 3 and Fig. 5b). The two motions preserve the same moving directions on the left flank of the entrance to the active site pocket, but differ in some other regions of the protein, including especially the long loop Phe 114–Asp 131 and a few C-terminal residues, where the motion is strong in the nitrated, and very weak in the native state. Together, the dominant motion in the Y135-nitrated complex seems to "behave" in compliance and not against

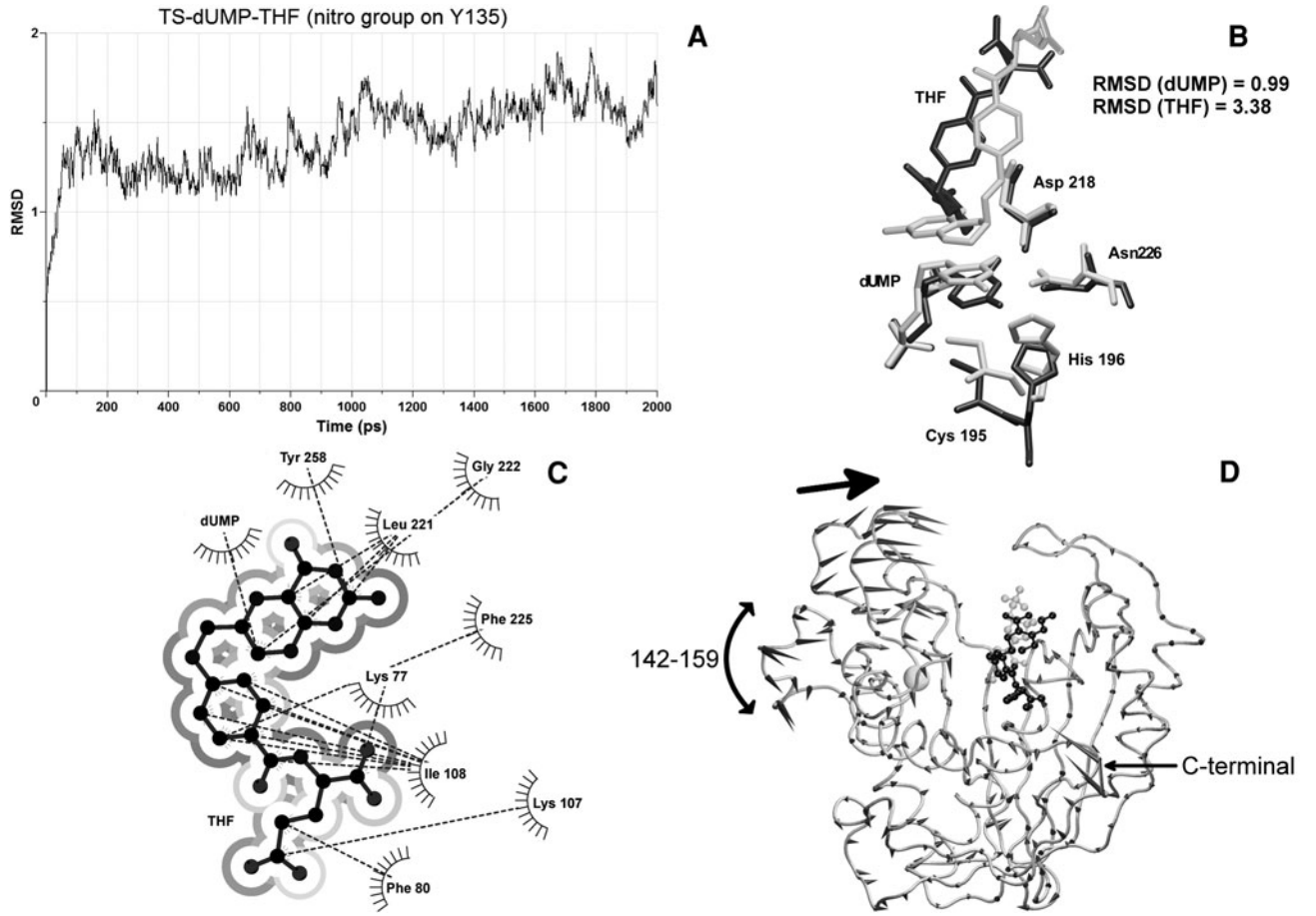

Fig. 7 **a** Time evolution of backbone RMSD (Å) from the structure after equilibration during 2,000 ps data collection MD simulation of (Y135-NO_2)hTS-dUMP-THF; **b** Superimposition of the average structures of hTS-dUMP-THF (*light*) and (Y135-NO_2)hTS-dUMP-THF (*dark*). Shown are the active site residues forming hydrogen bonds with the pyrimidine ring of dUMP, catalytic Cys 195, dUMP and THF. RMSDs (Å) are calculated for all heavy atoms in dUMP and THF. **c** LIGPLOT drawing of the hydrophobic interactions THF-dUMP and THF-protein in (Y135-NO_2)hTS-dUMP-THF. Solvent accessibility around the THF molecule is shown in *gray scale* from brightest (highly accessible atoms) to darkest (buried atoms); **b** and **c** Hydrogen atoms are omitted for clarity; **d** Concerted motions associated with the first eigenvector in (Y135-NO_2)hTS-dUMP-THF. dUMP and THF are shown respectively as *light* and *dark ball* and *sticks*. Tyr 135 is shown as a *sphere*. Concerted motions are shown as *cones* representing the product of the first eigenvector and first eigenvalue

the catalytic action of hTS, which is in contrary to the situation in the Y33-nitrated complex, discussed earlier in the manuscript.

Verdict Regardless of the dynamics of the protein appearing as not unfavorable, nitration on Y135 is expected to very strongly reduce or even eliminate the enzymatic activity of hTS.

Considering an overall unstable character of the RMSD curve from the 2 ns simulation of the (Y135-NO_2)hTS-dUMP-THF complex (Fig. 7b), this simulation was prolonged to 6 ns in search of stabilization of RMSD and to ascertain the results. However, reaching the 6th ns, the simulation was still not satisfactory stable, with the RMSD showing the lack of convergence. We observed that this behavior was due to a short distance between the nitration site on Y135 and the positions of ligands, dUMP and THF (see Table 6), resulting in strong electrostatic interactions between the nitro group of Y135 and the charged groups of ligands, leading to a periodic half-turn of the pterine ring of THF and coupled conformational change of several protein residues surrounding the binding site of the THF molecule (see also earlier discussion in this section on the mechanism of influence of Y135-nitration on the conformation of TS ligands). This behavior, however, does not affect the main results presented herein, as the binding position of THF and the alignment between THF pterine and dUMP pyrimidine rings are influenced similarly strong for both conformations of the THF molecule, leading to a prediction of a very strong reduction or even loss of enzymatic activity of human thymidylate synthase. RMSD plot from the 6-ns MD simulation and figure showing an alternative conformation of the THF molecule in the active site of the

(Y135-NO_2)hTS-dUMP-THF complex have been deposited as supplementary material.

Nitration on Y213

Superimposition of the average structures of the hTS-dUMP-THF and (Y213-NO_2)hTS-dUMP-THF complexes shows that the binding positions of both dUMP and THF are different in the latter compared to the former complex (Fig. 8b). The shift in the positions of the pyrimidine ring of dUMP and pterine ring of THF is similar for both rings in that the rings preserve an almost parallel alignment with respect to each other. The latter is reflected in the H-bonding network connecting the pyrimidine ring and neighboring protein residues (Table 5), which is closely similar in the nitrated and native complexes, but adjusts to the change in the position of the pyrimidine ring in the nitrated complex with an 19.2 % occurrence of the H-bond between Tyr 135 and pyrimidine O4, compared to an almost non-existing occurrence of this H-bond (0.3 %) in the native complex. It is also shown in a similar C5 (dUMP)–N5 (THF) distance (in fact, even shorter by 0.46 Å) in the nitrated compared to native state (Table 6). The new position of the THF molecule is maintained through several hydrophobic contacts between the PABA and pterine rings and the protein residues of Ile 108, Leu 221, Phe 225 and Trp 109, as well as a pair of hydrogen bonds between two nitrogen atoms (N1 and N2) of the pterine ring and Asn 112 (Fig. 8c). In addition, the thorough hydrophobic interface between the pterine and pyrimidine rings adds significantly to the overall stabilization of both rings.

The free energies of binding are unfavorable for the binding of dUMP (by about 3 kcal/mol) and THF (by about 0.9 kcal/mol) in the Y213-nitrated compared to native complex (Table 4). These results are somewhat surprising (especially the 3 kcal/mol disadvantage for the binding of dUMP), considering the apparently good stabilization of both ligands observed upon structural analysis of the nitrated state, discussed in the previous paragraph. This 3 kcal/mol free energy loss results apparently from the shifted position of the dUMP molecule, even in spite of all hydrogen bonds of the substrate (including those formed by the pyrimidine, ribose and phosphate) being preserved (as in the native complex). Inspection of the free energy contributions indicates that the binding of dUMP in the native state is preferred due to a favorable imbalance in the electrostatic pool of energies (see ΔE_{ele}, ΔG_{GB} and $\Delta G_{GB,ele}$ in Table 4), and the binding of THF—due to more favorable ΔE_{vdW} contributions and despite an unfavorable imbalance in $\Delta G_{GB,ele}$.

The dominant concerted motion in (Y213-NO_2)hTS-dUMP-THF, shown in Fig. 8d, is analogous and suppressed compared to the corresponding motion in the native system (cnf. Table 3 and Fig. 5b). Although these characteristics, and especially the former one, could suggest otherwise, but based upon the visual appearance of the motion in the Y213-nitrated system, the latter motion seems neutral, i.e., neither in accord, nor the opposite, with the catalytic function of the enzyme. In fact, the motion is weak (suppressed) to similar extent throughout the structure, showing no apparent signs of a possible functional effect.

The apparent controversy of this case (the results/observations from structural, energetic and dynamic analyses do not add up to a coherent picture) and the fact that Tyr 213 is located specifically in the interface region between the two identical monomeric subunits of hTS, with the latter location potentially affecting interactions between the monomeric subunits and thus being of potential relevance to the enzyme activity [42], prompted us to carry out simulation of the dimeric form of the Y213-nitrated protein. In accordance with the simulation protocols described in "Methods: Molecular dynamics (MD)" we performed two additional 2,000 ps MD simulations of the dimeric forms of hTS-dUMP-THF and (Y213-NO_2)hTS-dUMP-THF systems, with the active sites in monomeric subunits A and B occupied with dUMP and THF or lacking them, respectively, and the nitro groups present in both monomeric subunits of the nitrated system. The superimposition of the average structures from both simulations is shown in Fig. 9. The molecules of dUMP and THF show very similar positions of their pyrimidine and pterine rings, respectively, in both structures. The RMSDs of the heavy atoms of dUMP and THF with reference to the native complex are 0.75 and 2.55 Å, respectively, compared to slightly higher values of 0.97 and 2.75 Å, respectively, from the monomeric simulation of (Y213-NO_2)hTS-dUMP-THF. The parallel alignment between the pyrimidine and pterine rings is preserved in the Y213-nitrated compared to native system. This is reflected in similar hydrogen bonding and hydrophobic contacts patterns in both structures (not shown). The C6 (dUMP)–γS (Cys 195) and C5 (dUMP)–N5 (THF) distances are also similar in both structures, yet even shorter in the nitrated state, where they amount to 3.37 and 3.83 Å, respectively, compared to 3.50 and 4.20 Å, respectively, in the native state. The dimer interface region (composed mostly of the five central β-sheets from each monomeric subunit; Fig. 1) has changed little in the nitrated compared to native system as reflected in the backbone RMSD of 0.50 Å. These results speak for the activity of hTS being possibly unaffected upon the nitration of Tyr 213, suggesting the presence of two nitrated sites in the binding interface to slightly improve the already quite "satisfactory" (almost parallel) alignment of the ligands, which was predicted in the case

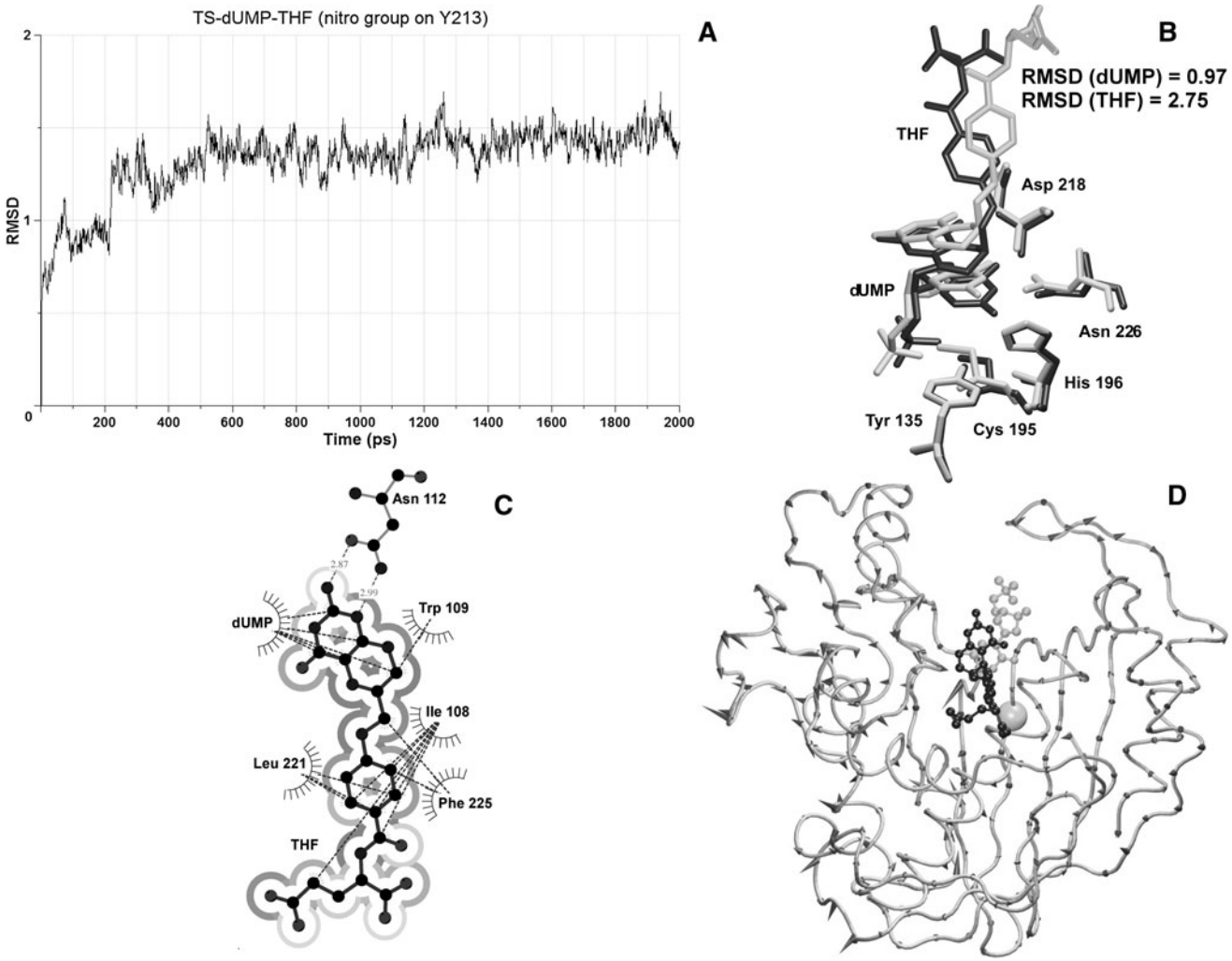

Fig. 8 **a** Time evolution of backbone RMSD (Å) from the structure after equilibration during 2,000 ps data collection MD simulation of (Y213-NO_2)hTS-dUMP-THF; **b** Superimposition of the average structures of hTS-dUMP-THF (*light*) and (Y213-NO_2)hTS-dUMP-THF (*dark*). Shown are the active site residues forming hydrogen bonds with the pyrimidine ring of dUMP, catalytic Cys 195, dUMP and THF. RMSDs (Å) are calculated for all heavy atoms in dUMP and THF. **c** LIGPLOT drawing of the hydrophobic interactions THF-dUMP and THF-protein in (Y213-NO_2)hTS-dUMP-THF. Solvent accessibility around the THF molecule is shown in *gray scale* from brightest (highly accessible atoms) to darkest (buried atoms); **b** and **c** Hydrogen atoms are omitted for clarity; **d** Concerted motions associated with the first eigenvector in (Y213-NO_2)hTS-dUMP-THF. dUMP and THF are shown respectively as *light* and *dark ball* and *sticks*. Tyr 213 is shown as a *sphere*. Concerted motions are shown as *cones* representing the product of the first eigenvector and first eigenvalue

of single (monomeric) nitration (Fig. 8b). However, the results of dimeric simulations should be treated as preliminary and we feel the case needs yet further, more comprehensive investigation including simulations of dimeric systems with both active sites occupied with ligands, one nitrated site per dimer, trajectory post-processing analyses, etc. It is worth of note that all other nitrated sites studied herein are located outside the interface region and at least comparably far from the interface than from the binding sites of dUMP and THF (Fig. 1), so their effect could neither be expected to affect monomer–monomer interactions comparably strong as the Y213-nitration, nor to influence the enzyme activity more from affecting the dimer interface than the positions of dUMP and THF. Therefore, simulations of dimeric systems other than the one nitrated on Y213 were not planned nor performed.

Verdict Nitration on Y213 is expected to affect the enzymatic activity of hTS very little or even not at all. However, this conclusion is not fully supported by the present results and this case is worth of further investigation.

Nitration on Y230

Superimposition of the average structures of hTS-dUMP-THF and (Y230-NO_2)hTS-dUMP-THF indicates different

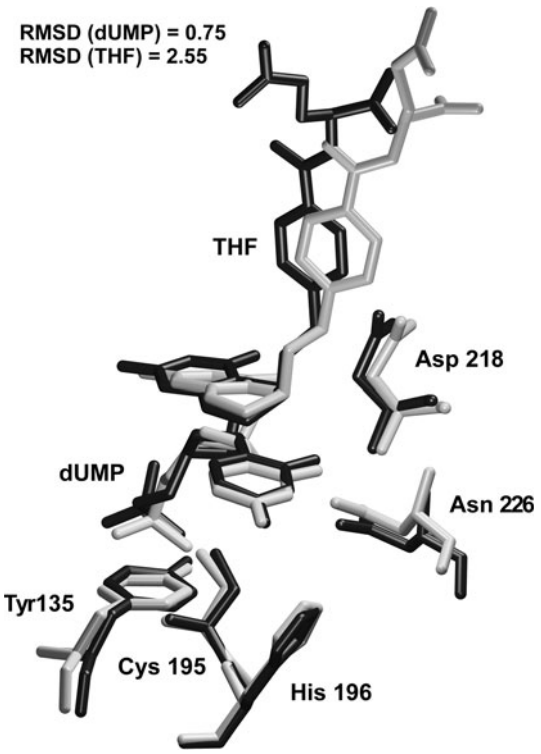

Fig. 9 Superimposition of the average dimer structures of hTS-dUMP-THF (*light*) and (Y213-NO_2)hTS-dUMP-THF (*dark*). Shown are selected residues in the active site of subunit A: amino acids forming hydrogen bonds with the pyrimidine ring of dUMP, catalytic Cys 195, dUMP and THF. Hydrogen atoms are omitted for clarity. RMSDs (Å) are calculated for all heavy atoms in dUMP and THF

binding positions of dUMP (moderate change) and THF (substantial change) (Fig. 10b). The pyrimidine ring of dUMP is shifted and slightly twisted in the nitrated compared to native complex. In the consequence of the shift, the ring gains, although only partially in the simulation, hydrogen bonds between O4 and the residues of Tyr 135 and His 196 (Table 5). Even despite the shift, though, the ring preserves majorly in the simulation the hydrogen bonds between O4, O2 and N(3)-H and the protein residues of Asn 226 and Asp 218. The new position of THF is maintained through a series of hydrophobic contacts between the PABA ring and Ile 108 and two contacts between the pterine ring and Leu 221 (Fig. 10c). The pterine ring is strongly rotated and moderately shifted away, relative to the pyrimidine ring, resulting in the loss of favorable pterine-pyrimidine whole-ring-stacking interaction, with only a few single hydrophobic contacts between the rings preserved. Apart from this overall very limited hydrophobic interface, the THF molecule is stabilized in the new binding position via hydrogen bonds between the two glutamate carboxylic groups and the protein residues of Lys 107, Arg 78 and Lys 77, as well as between certain heterocyclic atoms of the pterine ring and the Asp 218 and Gly 222 residues. Overall, the stabilization of the ligands in the active site of the Y230-nitrated complex is weaker, yet comparable with the native complex. However, a strong shift of the pterine ring and the resulting lack of the correct parallel alignment between this and the pyrimidine rings lessens the chances for the occurrence of the catalytic reaction. The latter is also reflected by the C5 (dUMP)–N5 (THF) distance being considerably longer in the nitrated compared to native state (cnf. Table 6).

The free energies of binding are unfavorable by about 2.2 kcal/mol for dUMP and 2.4 kcal/mol for THF in the Y230-nitrated compared to native complex (Table 4). These results are in qualitative agreement with the observations from structural analysis. Inspection of the free energy terms indicates that the binding of dUMP in the native state is favored compared with the nitrated state due to more favorable $\Delta G_{GB,ele}$ (balancing more favorable ΔE_{ele} with more unfavorable ΔG_{GB}) and ΔE_{vdW} contributions. The binding of THF in the native state is favored due to largely more favorable ΔE_{vdW} contributions, with the imbalance in $\Delta G_{GB,ele}$ strongly reducing the final difference in ΔG_{bind} by substantially favoring the nitrated state. The latter result confirms that the new position of THF in the nitrated state lacks a proper hydrophobic stabilization, this deficit being partially counterbalanced with a number of favorable H-bonding interactions between THF and neighboring polar amino acid residues (reflected in ΔE_{vdW} and $\Delta G_{GB,ele}$, respectively).

The dominant concerted motion in (Y230-NO_2)hTS-dUMP-THF, shown in Fig. 10d, is very poorly correlated, and strongly extended, relative to the corresponding motion in the native complex (cnf. Table 3 and Fig. 7). The motion is strongly asymmetric, being relatively large in approximately one half and very weak in the other half of the structure (right and left sides in Fig. 10d, respectively). The broad region where the motion is strong, encompasses, among many others, several residues paving the active site cleft, which play a role in hydrophobic stabilization of the PABA and pterine rings of THF (Phe 80, Ile 108, Trp 109, Leu 221, Gly 222, Phe 225). Their movement appears to influence the position of THF by partially "withdrawing" the hydrophobic stabilization (except from the contributions from Ile 108 and Leu 221) and thus causing the cofactor molecule to search for compensation elsewhere.

Verdict Nitration on Y230 is expected to significantly reduce the enzymatic activity of hTS.

Nitration on Y258

Superimposition of the average structures of hTS-dUMP-THF and (Y258-NO_2)hTS-dUMP-THF reveals similar binding positions of dUMP, and substantially different of THF (Fig. 11b). As for dUMP, while positions of the

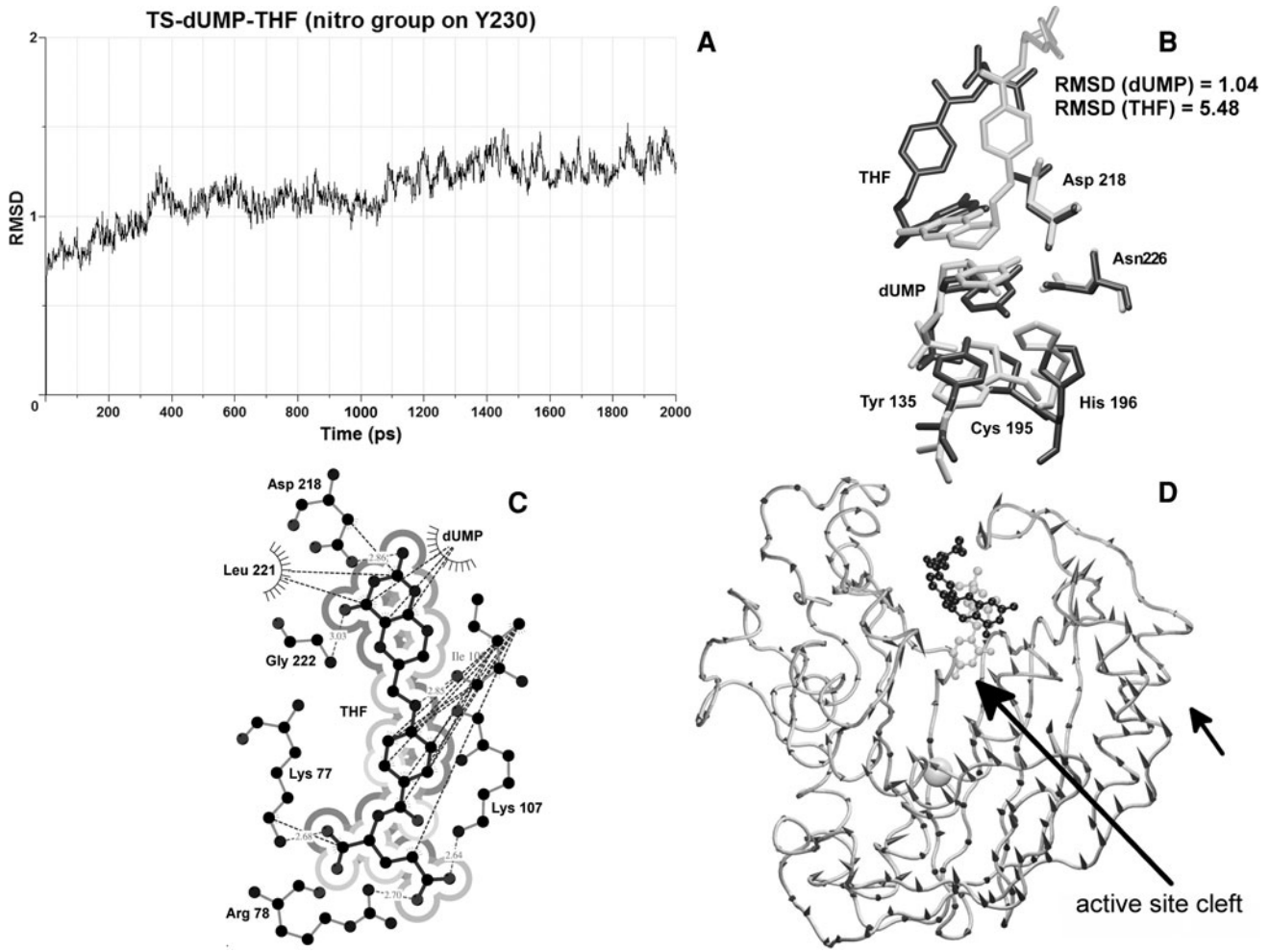

Fig. 10 **a** Time evolution of backbone RMSD (Å) from the structure after equilibration during 2,000 ps data collection MD simulation of (Y230-NO_2)hTS-dUMP-THF; **b** Superimposition of the average structures of hTS-dUMP-THF (*light*) and (Y230-NO_2)hTS-dUMP-THF (*dark*). Shown are the active site residues forming hydrogen bonds with the pyrimidine ring of dUMP, catalytic Cys 195, dUMP and THF. RMSDs (Å) are calculated for all heavy atoms in dUMP and THF. **c** LIGPLOT drawing of the hydrophobic interactions THF-dUMP and THF-protein in (Y230-NO_2)hTS-dUMP-THF. Solvent accessibility around the THF molecule is shown in *gray scale* from brightest (highly accessible atoms) to darkest (buried atoms); **b** and **c** Hydrogen atoms are omitted for clarity; **d** Concerted motions associated with the first eigenvector in (Y230-NO_2)hTS-dUMP-THF. dUMP and THF are shown respectively as *light* and *dark ball* and *sticks*. Tyr 230 is shown as a *sphere*. Concerted motions are shown as cones representing the product of the first eigenvector and first eigenvalue

pyrimidine ring are almost the same, those of ribose and phosphate are slightly different. Despite this level of similarity, the pyrimidine ring in the Y258-nitrated system maintains (majorly) in the simulation not only the hydrogen bonds from O4 and N3-H to Asn 226 but also, although at much lower occupancies, from O4 to the residues of His 196 and Tyr 135 (Table 5), the side chains of which are positioned slightly closer and favorably rotated relative to O4, as can be seen in the superimposition in Fig. 11b. On the other hand, the occupancy of the O2-Asp 218 H-bond is by more than 30 % lower in the nitrated compared to native state. The binding position of THF is stabilized less in the nitrated compared to native complex, as reflected by only a moderate hydrophobic interface connecting the cofactor rings with the protein residues of Leu 221, Ile 108, Trp 109 and Phe 80 in the former complex (Fig. 11c). This interface concerns almost exclusively the PABA ring, whereas the pterine ring shows only one single contact connecting the C7 atom and Trp 109. Moreover, the pterine ring in the nitrated state is located nearly two times farther from the pyrimidine ring than in the native state (see also the C5 (dUMP)–N5 (THF) distances in Table 6), resulting in the loss of ring-stacking and thus significantly reducing the stabilization of both rings and their parent molecules. This unusual shift, however, allows the pterine ring to move closer to Tyr 258, to a position where its N3-H and N2-H_2 groups can form hydrogen bonds with the two oxygens of the nitro group of Tyr 258 (not shown in Fig. 11c). In

addition, the binding position of THF is stabilized by two hydrogen bonds between the O4 atom of the pterine ring and Gly 222, and the glutamate alpha carboxylic group and Arg 78.

Free energies of binding are strongly unfavorable for the binding of dUMP (by about 9 kcal/mol) and THF (by about 3 kcal/mol) in the (Y258-NO_2)hTS-dUMP-THF compared to hTS-dUMP-THF complex (Table 4). These data are in accordance with the observations from the structural analysis, except that the difference between the binding free energies of dUMP seems overestimated. Inspection of the free energy contributions indicates that the bindings of dUMP and THF are favored in the native compared to nitrated complex, due to favorable ΔE_{vdW} and $\Delta G_{GB,ele}$, and much more favorable ΔE_{vdW} that overbalances unfavorable $\Delta G_{GB,ele}$, respectively. The less favorable stabilization of THF in the nitrated compared to native state, resulting from the much less favorable ΔE_{vdW} contributions in the former state, reflects considerably lowered hydrophobic stabilization of the cofactor molecule in the nitrated state, as discussed in the previous paragraph.

The dominant concerted motion in (Y258-NO_2)hTS-dUMP-THF, shown to the left in Fig. 11d, is analogous and equally strong compared to the corresponding motion in hTS-dUMP-THF (cnf. Table 3 and Fig. 5b). This motion does not seem relevant to the catalytic function of the enzyme. On the other hand, the motion along the second eigenvector, shown to the right in Fig. 11d, seems likely to have such relevance. The latter motion, which explains 10.1 % of the total variance in the dynamics of the nitrated system, is of relatively large magnitude at both (and especially the left one) flanks of the entrance to the active

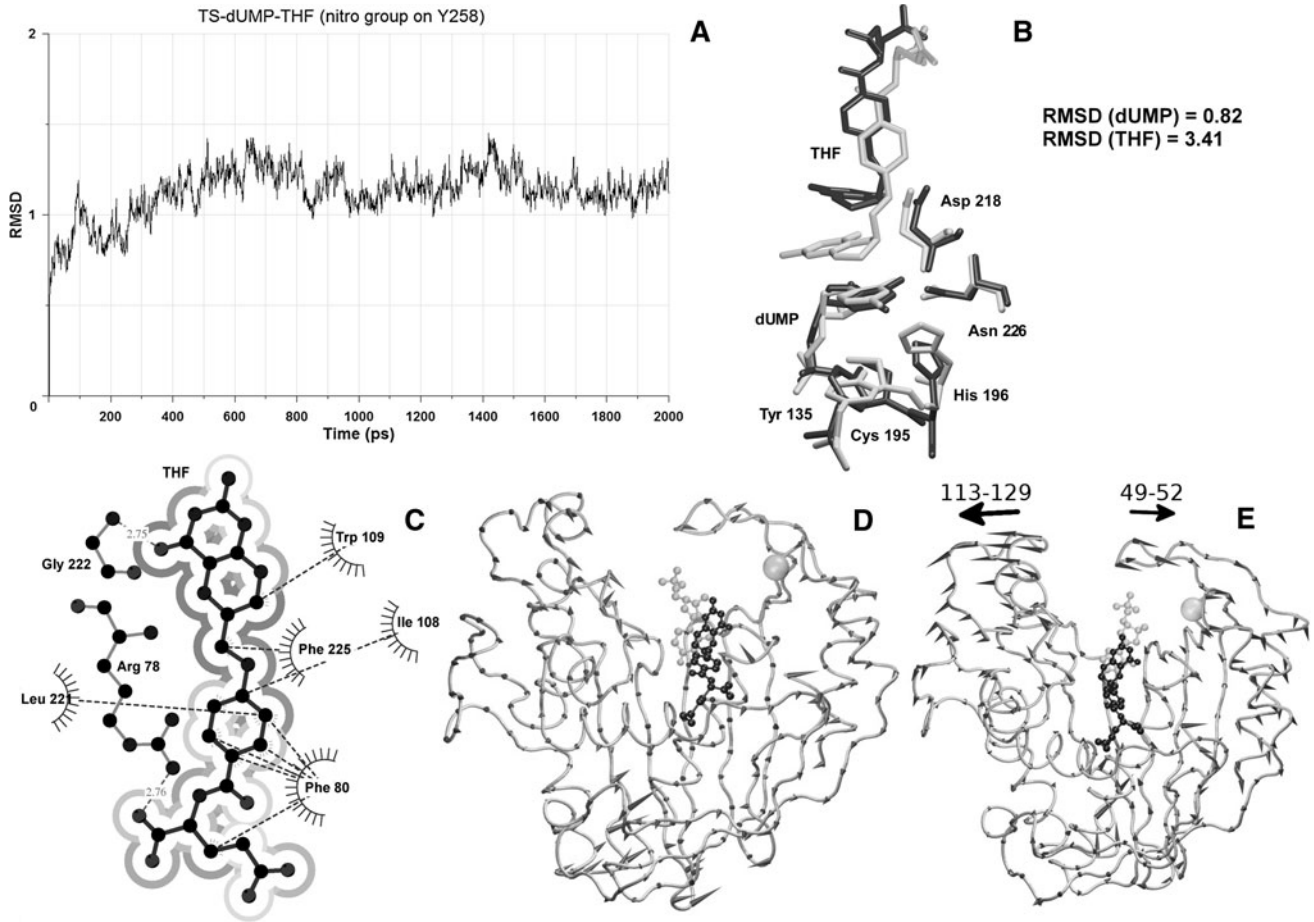

Fig. 11 **a** Time evolution of backbone RMSD (Å) from the structure after equilibration during 2,000 ps data collection MD simulation of (Y258-NO_2)hTS-dUMP-THF; **b** Superimposition of the average structures of hTS-dUMP-THF (*light*) and (Y258-NO_2)hTS-dUMP-THF (*dark*). Shown are the active site residues forming hydrogen bonds with the pyrimidine ring of dUMP, catalytic Cys 195, dUMP and THF. RMSDs (Å) are calculated for all heavy atoms in dUMP and THF. **c** LIGPLOT drawing of the hydrophobic interactions THF-dUMP and THF-protein in (Y258-NO_2)hTS-dUMP-THF. Solvent accessibility around the THF molecule is shown in *gray scale* from brightest (highly accessible atoms) to darkest (buried atoms); **b** and **c** Hydrogen atoms are omitted for clarity; **d** and **e** Concerted motions associated with the first (**d**) and second (**e**) eigenvectors in (Y258-NO_2)hTS-dUMP-THF. dUMP and THF are shown respectively as light and dark ball and sticks. Tyr 258 is shown as a *sphere*. Concerted motions are shown as *cones* representing the product of the eigenvectors and the corresponding eigenvalues

site pocket, where it extends to the outside of the pocket. This is demonstrated by an elongated distance of 15.1 Å between the Cα atoms of Ser 120 and Gly 52, compared to 10.2 Å in the native system. It suggests that the Y258-nitration may hinder the transition to the closed hTS conformation in the course of the formation of the active enzyme-substrate-cofactor complex.

Of note is that expression of the enzyme carrying Y258F mutation conferred FdUrd resistance to *E. coli* χ2913 cells, resulting probably from weaker inhibition of the mutated thymidylate synthase by FdUMP [43].

Verdict Nitration on Y258 is expected to very strongly reduce or even eliminate the enzymatic activity of hTS.

Nitration on Y301

Superimposition of the average structures of hTS-dUMP-THF and (Y301-NO_2)hTS-dUMP-THF, shown in Fig. 12b, reveals the binding positions of dUMP to be similar, with the positions of THF being very different. In particular, the positions of the pyrimidine ring of dUMP are virtually the same in the both structures. The latter is reflected in very similar patterns of hydrogen bonding, i.e. the occupancies of the H-bonds between O2 and Asp 218, and N3-H and O4 and Asn 226 are preserved majorly in the simulations and to similar extents in the two complexes (Table 5). No other hydrogen bonds with the pyrimidine ring in the nitrated state were present in the simulation. The pterine and PABA rings of THF in the nitrated complex are strongly shifted away from their positions in the native complex, with the glutamate moieties occupying similar (partially overlapping) positions in both complexes. The new positions of the pterine and PABA rings are stabilized with a series of hydrophobic contacts with the protein residues of Leu 221, Trp 109, Ile 108 and Phe 225 (Fig. 12c). This hydrophobic interface is moderately extensive, lacking contacts to two carbon atoms (C7 and C8A) of the pterine ring. In addition, the pterine ring lacks the ring-stacking interaction with the pyrimidine ring of dUMP, causing lack of stabilization (due to this effect) for both rings. On the other hand, stabilization of the THF molecule increases due to its several hydrogen bonds with the protein residues of Asp 218, Lys 77, Lys 107 and Arg 78. The C6 (dUMP)–γS (Cys 195) and C5 (dUMP)–N5 (THF) distances are 3.79 and 4.36 Å, respectively, both longer (by 0.19 and 0.34 Å, respectively) than in the native complex (cnf. Table 6).

Free energies of binding are unfavorable for the binding of dUMP and THF (by about 8.6 and 1.2 kcal/mol, respectively) in the (Y301-NO_2)hTS-dUMP-THF compared to hTS-dUMP-THF complex (Table 4). These data are in accord with the observations from structural analysis, although, similar to the case of Y258-nitrated complex, the difference in the binding free energy of dUMP between the two states (nitrated and native) seems likely overestimated. Inspection of the free energy terms shows that the bindings of dUMP and THF are disfavored in the nitrated, compared to native state, due to less favorable $\Delta G_{GB,ele}$ and ΔE_{vdW} contributions, and substantially less favorable ΔE_{vdW} that is not fully counterbalanced by more favorable $\Delta G_{GB,ele}$, respectively.

The dominant concerted motion in (Y301-NO_2)hTS-dUMP-THF, shown in Fig. 12d, is very poorly correlated, and slightly suppressed, compared to the corresponding motion in hTS-dUMP-THF (cnf. Table 3 and Fig. 5b). The motion is relatively strong on the left flank of the entrance to the active site pocket, where it extends to the outside of the pocket, resulting in the elongation of distances between the both flanks (for example, 12.9 Å between the Cα atoms of Ser 120 and Gly 52, compared to 10.2 Å in the native system). The latter effect, observed also in the Y33- and Y258-nitrated complexes, has likely unfavorable influence on the catalytic function of hTS, as has been discussed earlier in the manuscript.

Verdict Nitration on Y301 is expected to significantly reduce the enzymatic activity of hTS.

This verdict deserves an additional comment, since nitration on Y301 is the most distant one in the examined series (cnf. Table 6). Its predicted strong influence on the activity of hTS can be explained in view of the electrostatic repulsion between the γ-carboxylic group of the glutamate portion of THF and the nitro group on Y301. This repulsion interaction is likely strong, and thus capable of remodeling the shape of the THF molecule, due to relatively close distance of about 9.9 Å between the interacting groups, which is much shorter compared to the distance of about 20.2 Å between the nitro group on Y301 and the centroid of the pterine ring in THF. The latter difference results from a specific structural arrangement between the tyrosine 301 and THF moieties, which are extended toward each other, with the substituents of phenolic ring (–OH, –NO_2) on the one side, and the γ-carboxylic group on the other side, being the closest ends in this arrangement.

Considering the residue of Y301 lying in the proximity of the C-terminus and that the 1I00 structure, which served as a starting model in the simulations, is missing seven C-terminal residues that are present in the hTS sequence, control simulations were carried out to assess if the presence of the complete C-terminus could affect the results. The missing C-terminal residues were derived from the superimposed structure of another hTS-dUMP-Tomudex complex (PDB ID: 1HVY [44]). Structural results of the 2,000 ps simulations of the native and Y301-nitrated structures with complete C-termini (structures I00-HVY and (Y301-NO_2)I00-HVY, respectively) were in sound agreement with the results of the corresponding simulations of the structures with incomplete C-termini (hTS-

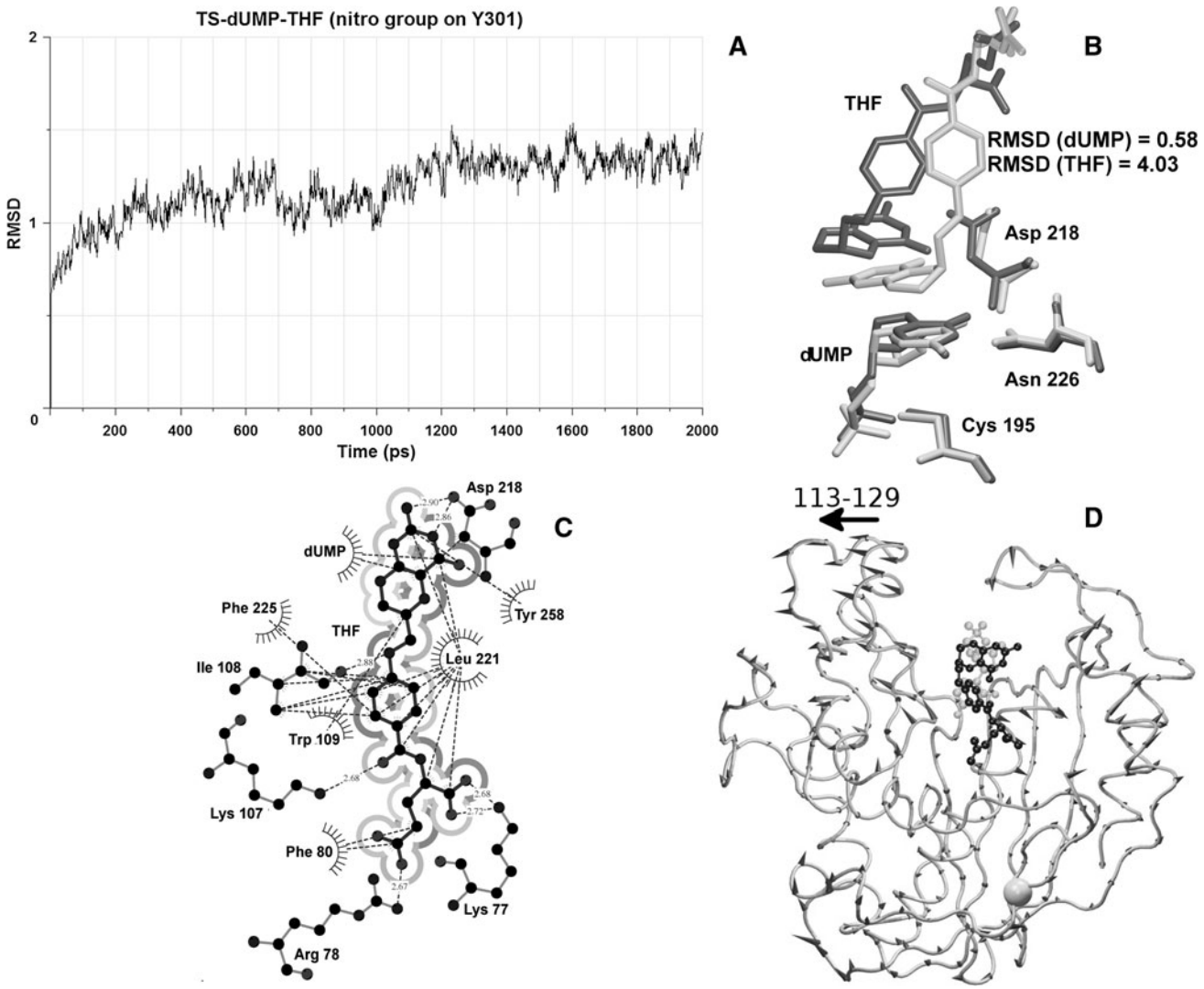

Fig. 12 **a** Time evolution of backbone RMSD (Å) from the structure after equilibration during 2,000 ps data collection MD simulation of (Y301-NO_2)hTS-dUMP-THF; **b** Superimposition of the average structures of hTS-dUMP-THF (*light*) and (Y301-NO_2)hTS-dUMP-THF (*dark*). Shown are the active site residues forming hydrogen bonds with the pyrimidine ring of dUMP, catalytic Cys 195, dUMP and THF. RMSDs (Å) are calculated for all heavy atoms in dUMP and THF. **c** LIGPLOT drawing of the hydrophobic interactions THF-dUMP and THF-protein in (Y301-NO_2)hTS-dUMP-THF. Solvent accessibility around the THF molecule is shown in *gray scale* from brightest (highly accessible atoms) to darkest (buried atoms); **b** and **c** Hydrogen atoms are omitted for clarity; **d** Concerted motions associated with the first eigenvector in (Y301-NO_2)hTS-dUMP-THF. dUMP and THF are shown respectively as *light* and *dark ball* and *sticks*. Tyr 301 is shown as a *sphere*. Concerted motions are shown as *cones* representing the product of the eigenvectors and the corresponding eigenvalues

dUMP-THF and (Y301-NO_2)hTS-dUMP-THF, respectively). The molecules of dUMP and THF showed similar relative positions of their pyrimidine and pterine rings, respectively, in both pairs of structures, with the (Y301-NO_2)I00-HVY structure lacking the parallel alignment and the pyrimidine-pterine ring-stacking (not shown) analogously as the (Y301-NO_2)hTS-dUMP-THF structure (Fig. 12b). The RMSDs of the heavy atoms of dUMP and THF were 0.95 and 4.83 Å, respectively, for the nitrated with respect to native complexes with complete C-termini, compared to moderately lower values of 0.58 and 4.03 Å, respectively, for the corresponding complexes with incomplete C-termini. The hydrogen bonding and hydrophobic contacts with ligands were also similar between the corresponding complexes in both pairs of structures. In the I00-HVY and (Y301-NO_2)I00-HVY complexes, the prolonged C-terminus showed a larger backbone RMSD of 3.12 Å, compared to a moderate backbone RMSD of 1.28 Å for the entire protein. Nevertheless, the active sites remained open to similar extent in the structures with complete, compared to the corresponding structures with incomplete, C-termini, with the latter effect likely arising

from the open conformation of the 1I00 structure, being the major component of the I00-HVY model. Together, the control simulations reinforced the verdict derived from the simulation of the (Y301-NO_2)hTS-dUMP-THF structure, showing the additional residues at the C-terminus did not affect the predicted effect on the enzymatic activity exerted by the nitro group on Y301.

Conclusions

In the present paper, we perform molecular dynamics, essential dynamics and free energy computations in order to anticipate, based on changes in structure, dynamics and binding free energies, effects of each MS-revealed nitration on the enzymatic activity of hTS. The above mentioned computational approach has already been successfully used by us in studies of the effect of lowered catalytic activity of the hTS enzyme caused by another post-translational modification, phosphorylation, of Ser 124 residue, being distant from the active site [17]. Approaches employing molecular dynamics and MD-based methods have been demonstrated to be helpful in elucidating molecular mechanisms of various phenomena caused by post-translational modifications (phosphorylation, nitration) in protein systems [17, 45–53]. Taking advantage of expanding computational resources, these atomistic approaches offer a convenient and efficient way to advance our understanding of PTMs: their functions and mechanisms of action. This is demonstrated in our paper, where the computational approach is used to explore the context build by experimental data, supplementing it with results on atomistic level, which broaden the scope of understanding of the investigated PTMs.

Our results indicate that most of the studied TS nitrations, including Y33, Y135, Y230, Y258 and Y301, have a strong detrimental effect on the enzymatic activity of hTS. Only two nitrations in the series, Y65 and Y213, appear to influence the enzymatic activity of hTS weakly, or even not at all. Therefore, an overall conclusion can be drawn that the MS-revealed tyrosine nitrations in the human TS enzyme show clear tendency to influence the structure and dynamics and, in turn, catalytic properties of the host enzyme. With one exception (see "Nitration on Y301"), this effect is distance-dependent, as it disappears or considerably lessens for the two modifications that are distantly located from the active site (Y65 and Y213; Table 6). Notably, although certain TS nitrations (e.g. Y33, Y135, Y230, Y258 and Y301) strongly affecting the enzyme activity cause distinct alterations of substrate binding positions, kinetic studies showed nitration to influence V_{max} rather than K_m values describing human thymidylate synthase reaction [15].

Acknowledgments Part of the computations was performed at the Interdisciplinary Center for Mathematical and Computational Modelling (ICM) of the Warsaw University, Poland. Supported by the Ministry of Science and Higher Education (grant No. NN401 0240 36).

References

1. Carreras CW, Santi DV (1995) The catalytic mechanism and structure of thymidylate synthase. Annu Rev Biochem 64: 721–762
2. Lehman NL (2002) Future potential of thymidylate synthase inhibitors in cancer therapy. Expert Opin Investig Drugs 11: 1775–1787
3. Ackland SP, Clarke SJ, Beale P, Peters GJ (2002) In: Giaccone G, Schilsky R, Sondel P (eds) Cancer chemotherapy and biological response modifiers. Elsevier, Amsterdam, pp 1–36
4. Jarmuła A (2010) Antifolate inhibitors of thymidylate synthase as anticancer drugs. Mini Rev Med Chem 10:1211–1222
5. Trujillo M, Alvarez B, Souza JM, Romero N, Castro L, Thomson L, Radi R (2000) In: Ignarro LJ (ed) Nitric oxide: biology and pathobiology, 1st edn. Academic Press, San Diego, pp 61–102
6. Yeo W-S, Lee SJ, Lee JR, Kim KP (2008) Nitrosative protein tyrosine modifications: biochemistry and functional significance. BMB Rep 41:194–203
7. Schopfer NJ, Baker PR, Freeman BA (2003) NO-dependent protein nitration: a cell signaling event or an oxidative inflammatory response? Trends Biochem Sci 28:646–654
8. Sekar Y, Moon TC, Slupsky CM, Befus AD (2010) Protein tyrosine nitration of aldolase in mast cells: a plausible pathway in nitric oxide-mediated regulation of mast cell function. J Immunol 185:578–587
9. Radi R (2004) Nitric oxide, oxidants, and protein tyrosine nitration. Proc Natl Acad Sci USA 23:4003–4008
10. Liu Z, Cao J, Ma Q, Gao X, Ren J, Xue J (2011) GPS-YNO2: computational prediction of tyrosine nitration sites in proteins. Mol BioSyst 7:1197–1204
11. Abello N, Kerstjens HAM, Postma DS, Bischoff R (2009) Protein tyrosine nitration: selectivity, physicochemical and biological consequences, denitration, and proteomics methods for the identification of tyrosine-nitrated proteins. J Prot Res 8: 3222–3238
12. Mikhailov VA, Iniesta J, Cooper HJ (2010) Top-down mass analysis of protein tyrosine nitration: comparison of electron capture dissociation with "slow-heating" tandem mass spectrometry methods. Anal Chem 82:7283–7292
13. Sacksteder CA, Qian WJ, Knyushko TV, Wang H, Chin MH, Lacan G, Melega WP, Camp DG 2nd, Smith RD, Smith DJ, Squier TC, Bigelow DJ (2006) Endogenously nitrated proteins in mouse brain: links to neurodegenerative disease. Biochemistry 45:8009–8022
14. Ghesquiere B, Colaert N, Helsens K, Dejager L, Vanhaute C, Verleysen K, Kas K, Timmerman E, Goethals M, Libert C, Vandekerckhove J, Gevaert K (2009) In vitro and in vivo protein-bound tyrosine nitration characterized by diagonal chromatography. Mol Cell Proteomics 8:2642–2652
15. Dąbrowska-Maś E, Frączyk T, Ruman T, Radziszewska K, Wilk P, Cieśla J, Zieliński Z, Jurkiewicz A, Gołos B, Wińska P, Wałajtys-Rode E, Leś A, Nizioł J, Jarmuła A, Stefanowicz P, Szewczuk Z, Rode W (2012) Tyrosine nitration affects thymidylate synthase properties. Org Biomol Chem 10:323–331
16. Almog R, Waddling CA, Maley F, Maley GF, Van Roey P (2001) Crystal structure of a deletion mutant of human thymidylate

synthase Delta (7–29) and its ternary complex with Tomudex and dUMP. Protein Sci 10:988–996
17. Jarmuła A, Frączyk T, Cieplak P, Rode W (2010) Mechanism of influence of phosphorylation on serine 124 on a decrease of catalytic activity of human thymidylate synthase. Bioorg Med Chem 18:3361–3370
18. Case DA, Darden TA, Cheatham TE III, Simmerling CL, Wang J, Duke RE, Luo R, Merz KM, Wang B, Pearlman DA, Crowley M, Brozell S, Tsui V, Gohlke H, Mongan J, Hornak V, Cui G, Beroza P, Schafmeister C, Caldwell JW, Ross WS, Kollman PA (2004) AMBER 8. University of California, San Francisco
19. Jorgensen WL, Chandrasekhar J, Madura JD, Impey RW, Klein ML (1982) Comparison of simple potential functions for simulating liquid water. J Chem Phys 79:926–935
20. Duan Y, Wu C, Chowdhury S, Lee MC, Xiong G, Zhang W, Yang R, Cieplak P, Luo R, Lee T (2003) A point-charge force field for molecular mechanics simulations of proteins based on condensed-phase quantum mechanical calculations. J Comput Chem 24:1999–2012
21. Wang J, Wolf RM, Caldwell JW, Kollman PA, Case DA (2004) Development and testing of a general amber force field. J Comput Chem 25:1157–1174
22. Bayly CI, Cieplak P, Cornell WD, Kollman PA (1993) A well-behaved electrostatic potential based method using charge restraints for determining atom-centered charges: the RESP model. J Phys Chem 97:10269–10280
23. Cieplak P, Cornell WD, Bayly CI, Kollman PA (1995) Application of the multimolecule and multiconformational RESP methodology to biopolymers: charge derivation for DNA, RNA and proteins. J Comput Chem 16:1357–1377
24. Ryckaert JP, Ciccotti G, Berendsen HJC (1977) Numeric integration of the Cartesian equations of motion of a system with constraints: molecular dynamics of n-alkanes. J Comput Phys 23:327–341
25. York DM, Darden TA, Pedersen LG (1993) The effect of long-range electrostatic interactions in simulations of macromolecular systems—a comparison of the Ewald and truncated list methods. J Chem Phys 99:8345–8348
26. Essmann U, Perera L, Berkowitz ML, Darden TA, Lee H, Pedersen LG (1995) A smooth particle mesh Ewald method. J Chem Phys 103:8577–8793
27. Wallace AC, Laskowski RA, Thornton JM (1995) LIGPLOT: a program to generate schematic diagrams of protein-ligand interactions. Protein Eng 8:127–134
28. Hubbard SJ, Thornton JM (1993) 'NACCESS', computer program. Department of Biochemistry and Molecular Biology, University College London, London
29. Amadei A, Linssen AB, Berendsen HJ (1993) Essential dynamics of proteins. Proteins 17:412–425
30. Amadei A, Linssen AB, de Groot BL, van Aalten DM, Berendsen HJ (1996) An efficient method for sampling the essential subspace of proteins. J Biomol Struct Dyn 13:615–625
31. Meyer T, Ferrer-Costa C, Perez A, Rueda A, Bidon-Chanal A, Luque FJ, Laughton CA, Orozco M (2006) Essential dynamics: a tool for efficient trajectory compression and management. J Chem Theor Comput 2:251–258
32. Haider S, Parkinson GN, Neidle S (2008) Molecular dynamics and principal component analysis of human telomeric quadruplex multimers. Biophys J 95:296–311
33. Kollman PA, Massova I, Reyes C, Kuhn B, Huo S, Chong L, Lee M, Lee T, Duan Y, Wang W, Donini O, Cieplak P, Srinivasan J, Case DA, Cheatham TE III (2000) Calculating structures and free energies of complex molecules: combining molecular mechanics and continuum models. Acc Chem Res 33:889–897
34. Tsui V, Case DA (2000) Molecular dynamics simulations of nucleic acids using a generalized Born solvation model. J Am Chem Soc 122:2489–2498
35. Tsui V, Case DA (2001) Theory and applications of the generalized Born solvation models in macromolecular simulations. Biopolymers 56:275–291
36. Weiser J, Shenkin PS, Still WC (1999) Approximate atomic surfaces from linear combinations of pairwise overlaps (LCPO). J Comput Chem 20:217–230
37. Weis A, Katebzadeh K, Söderhjelm P, Nilsson I, Ryde U (2006) Ligand affinities predicted with the MM/PBSA method: dependence on the simulation method and the force field. J Med Chem 49:6596–6606
38. Hou T, Wang J, Li Y, Wang W (2011) Assessing the performance of the MM/PBSA and MM/GBSA methods. 1. The accuracy of binding free energy calculations based on molecular dynamics simulations. J Chem Inf Model 51:69–82
39. Stroud RM, Finer-Moore JS (2003) Computational dynamics along an enzymatic reaction pathway: thymidylate synthase, "the movie". Biochemistry 42:239–247
40. Hughey CT, Barbour KW, Berger FG, Berger SH (1993) Functional effects of a naturally occurring amino acid substitution in human thymidylate synthase. Mol Pharmacol 44:316–323
41. Cardinale D, Salo-Ahen OMH, Guaitoli G, Ferrari S, Venturelli A, Franchini S, Battini R, Ponterini G, Wade RC, Costi MP (2010) Design and characterization of a mutation outside the active site of human thymidylate synthase that affects ligand binding. Protein Eng Des Sel 23:81–89
42. Cardinale D, Guaitoli G, Tondi D, Luciani R, Henrich S, Salo-Ahen OMH, Ferrari S, Marverti G, Guerrieri D, Ligabue A, Frassineti C, Pozzi C, Mangani S, Fessas D, Guerrini R, Ponterini G, Wade RC, Costi MP (2011) Protein-protein interface-binding peptides inhibit the cancer therapy target human thymidylate synthase. PNAS 108:E542–E549
43. Kawate H, Landis DM, Loeb LA (2002) Distribution of mutations in human thymidylate synthase yielding resistance to 5-fluorodeoxyuridine. J Biol Chem 277:36304–36311
44. Phan J, Koli S, Minor W, Dunlap RB, Berger SH, Lebioda L (2001) Human thymidylate synthase is in the closed conformation when complexed with dUMP and raltitrexed, an antifolate drug. Biochemistry 40:1897–1902
45. Lian P, Wei DQ, Wang JF, Chou KC (2010) An allosteric mechanism inferred from molecular dynamics simulations on phospholamban pentamer in lipid membranes. PLoS One 6:e18587
46. Lu SY, Jiang YJ, Zou JW, Wu TX (2011) Molecular modeling and molecular dynamics simulation studies of the GSK3β/ATP/substrate complex: understanding the unique P+4 primed phosphorylation specificity for GSK3β substrates. J Chem Inf Model 51:1025–1036
47. Khuntawee W, Rungrotmongkol T, Hannongbua S (2012) Molecular dynamic behavior and binding affinity of flavonoid analogues to the cyclin dependent kinase 6/cyclin D complex. J Chem Inf Model 52:76–83
48. Herrou J, Rostkoff G, Luo Y, Roux B, Crosson S (2012) Structural basis of a protein partner switch that regulates the general stress response of α-proteobacteria. Proc Natl Acad Sci USA. doi: 10.1073/pnas.1116887109
49. Cao Q, Wang XJ, Liu CW, Liu DF, Li LF, Gao YQ, Su XD (2012) Inhibitory mechanism of caspase-6 phosphorylation revealed by crystal structures, molecular dynamics (MD) simulations and biochemical assays. J Biol Chem 287:15371–15379
50. Dodson GG, Lane DP, Verma CS (2008) Molecular simulations of protein dynamics: new windows on mechanisms in biology. EMBO Rep 9:144–150

51. Narayanan A, Jacobson MP (2009) Computational studies of protein regulation by post-translational phosphorylation. Curr Opin Struct Biol 19:156–163
52. Moreno DM, Marti MA, De Biase PM, Estrin DA, Demicheli V, Radi R, Boechi L (2011) Exploring the molecular basis of human manganese superoxide dismutase inactivation mediated by tyrosine 34 nitration. Arch Biochem Biophys 507:304–309
53. Singh SR, Prakash S, Muneeswaran G, Rajesh S, Muthukumar K, Vasu V, Karunakaran C (2012) Molecular dynamics simulation studies on structural and conformational changes in tyrosine-67 nitrated cytochrome c. Mol Simulat 38:459–467
54. Humphrey W, Dalke A, Schulten K (1996) VMD: visual molecular dynamics. J Mol Graph 14(33–38):27–28